Marine Geology 254 (2008) 129–151

Contents lists available at ScienceDirect

Marine Geology

journal homepage: www.elsevier.com/locate/margeo

Paleodrainage on the Chukchi shelf reveals sea level history and meltwater discharge

Jenna C. Hill [a,b,*], Neal W. Driscoll [a]

[a] Scripps Institution of Oceanography, University of California San Diego, La Jolla, CA 92093, United States
[b] Burroughs & Chapin Center for Marine & Wetland Studies, Coastal Carolina University, Conway, SC, United States

ARTICLE INFO

Article history:
Received 30 April 2007
Received in revised form 16 May 2008
Accepted 27 May 2008

Keywords:
Chukchi Sea
seismic reflection
marine geology
stratigraphy

ABSTRACT

CHIRP subbottom data collected across the Chukchi shelf, offshore NW Alaska, imaged numerous paleochannels and valleys that appear to have been downcut and incised during sea level falls associated with glacial intervals. In contrast, the two most recent incisions appear to have been formed during the period of sea level rise following the Last Glacial Maximum (LGM). The architecture and infill associated with these two incisions suggests that they were formed by an increase in discharge. These events appear to be unrelated to sea level fluctuations, but rather triggered by climatic variations during the most recent deglaciation (i.e. meltwater discharge). Radiocarbon dates from sediment cores within the southern incised valley suggest that the two episodes of meltwater discharge may correlate with Meltwater Pulse 1-A (~14,000 cal. yr BP) and evidence of iceberg scouring on outer Chukchi shelf (~12,000 to 13,000 cal. yr BP), respectively. Regional transgression across the interfluves on the middle Chukchi shelf appears to postdate the second meltwater discharge and may correlate with Meltwater Pulse 1-B (11,500 cal. yr BP). This evidence suggests that in glacially dominated landscapes, episodes of large discharge to the shelf might be out of phase with the sea level cycle. In addition, the presence of glacial meltwater drainage on the shelf implies a greater volume of continental glaciation during the LGM than previously recognized.

1. Introduction

The Chukchi Sea overlies a broad, shallow shelf between northern Alaska and Siberia that has been repeatedly exposed during periods of lowered sea level (Fig. 1). CHIRP subbottom data imaged extensive buried paleochannel networks on the shelf offshore NW Alaska that appear to record several sea level falls. Incision and downcutting are often interpreted to occur as result of base level lowering (Christie-Blick and Driscoll, 1995); however, along glaciated margins fluctuations in discharge associated with glacial lake breaching, meltwater discharge and climatic oscillations can lead to renewed incision and downcutting independent of base level change. While most of the fluvially incised valleys observed on the Chukchi shelf appear to be related to variations in sea level, the two most recent incisions appear to represent glacial meltwater pulses. Similar observations have been made on other glaciated margins where glacial lake breaching has played an important role in shaping margin morphology (e.g., Uchupi et al., 2001 and references within). Glacial outburst floods from ice dammed lakes in southern New England produced sheet flows that deposited large sediment lobes across the New York–New Jersey margin and emplaced numerous large glacial erratics on the outer shelf (Uchupi et al., 2001). The Hudson Shelf Valley is also believed to have been incised by high discharge flows from glacial meltwater that scoured the channel, contributing to incision and sediment bypass (Uchupi et al., 2001; Donnelly et al., 2005). Massive floods from Glacial Lake Missoula carved the Channeled Scabland topography of Washington and induced hyperpycnal flows with turbidite deposits than can be traced more than 1000 km offshore (Bretz, 1969; Normark and Reid, 1998; Zuffa et al., 2000).

It is important to recognize how the morphology of glaciated margins differs from non-glaciated, temperate and low latitude regions in order to understand the processes that can lead to renewed incision and downcutting in the absence of base level lowering.

The channel formation and evolution presented in Hill et al. (2007) is expanded upon here, with additional CHIRP and Boomer subbottom data, as well as sediment core data and radiocarbon ages that corroborate the initial interpretations and place important constraints on channel development and drainage evolution across the Chukchi margin. Evidence presented here also implies a greater extent of glaciation than previously recognized (Brigham-Grette, 2001), which has important implications for development of global climate models (Smith et al., 2003; Zweck and Huybrechts, 2005), the understanding of freshwater balances in the Arctic (Aagard and Carmack, 1989) and the degree of climate variability across the region (Keigwin et al., 2006).

* Corresponding author. Burroughs & Chapin Center for Marine & Wetland Studies, Coastal Carolina University, P.O. Box 261954, Conway, SC 29528, United States. Tel.: +1 843 349 4027; fax: +1 843 349 4042.
E-mail address: jchill@coastal.edu (J.C. Hill).

0025-3227/$ – see front matter © 2008 Elsevier B.V. All rights reserved.
doi:10.1016/j.margeo.2008.05.018

2. Regional setting

2.1. Tectonics

The complex tectonic history of Arctic Alaska and the surrounding shelves is comprised of a number of rifting, subduction and uplift events (Moore et al., 1994). Uplift in the mid-Jurassic to late Cretaceous produced much of the modern topography observed in northern Alaska. The Barrow Arch, which forms a broad structural high trending along the Beaufort coast, developed as a result of the late Cretaceous rifting that opened the Canada Basin (Fig. 2) (Moore et al., 1994). Around the same time, subduction of the Arctic Terrane along the northern margin transitioned into uplift along the northward verging Brooks Range thrust zone and the southern flank of the Barrow Arch became the foreland basin for the nascent orogenic belt (Moore et al., 1994). The E–W trending Brooks Range dominates the modern topography and exposed imbricate folds of the northern foothills transition into the broad, flat topography of the Arctic Coastal Plain that comprises most of the North Slope.

Offshore, uplift along the Herald thrust has created a structural high that separates the northwestern Chukchi margin from the Hope Basin to the south (Fig. 2). The NE verging Herald thrust trends NW–SE across the Chukchi shelf and converges with the Brooks Range thrust on the Lisburne Peninsula in the Chukchi syntaxis (Moore et al., 2002). On the northern side of the Herald Arch, the Hanna wrench fault zone, a complex, north trending, failed rift basin, covers a large portion of the northwestern shelf, while a series of listric normal faults related to rifting along the Beaufort margin makes up the North Chukchi Basin in the east (Thurston and Theiss, 1987). The Hope Valley to the south is a an extensional drop-down basin made up of half-grabens that originated through transtension on a dextral-slip fault system in the Eocene (Tolson, 1987).

2.2. Drainage patterns

The Brooks Range is the drainage divide for northern Alaska. Most of the southwestern foothill drainage flows through Kotzebue Sound into the Chukchi Sea, while the northern foothills predominantly discharge into the Beaufort Sea. The primary modern drainage in northern Alaska flows NNE through the Colville River, while the southern Brooks Range drains through Hope Valley. The Colville River drains a large portion of the North Slope (~60,000 km^2; Lamke et al., 1995) and flows axial parallel through much of the foreland basin of

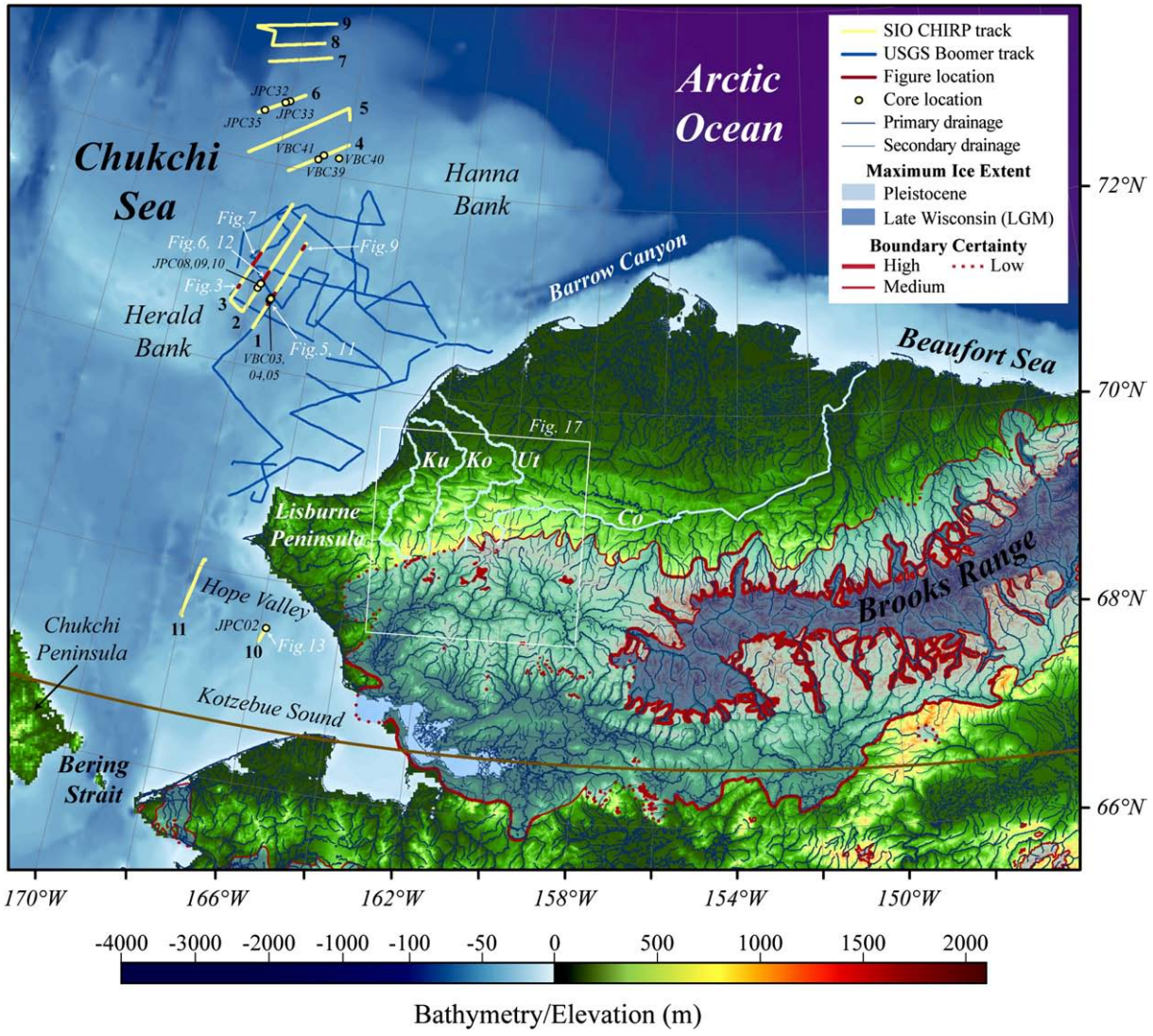

Fig. 1. Location map of northern Alaska and the adjacent Chukchi margin showing SIO CHIRP and USGS Boomer subbottom tracks. CHIRP profile numbers are labeled in bold and piston core locations are also noted. Figure profiles discussed in the text are highlighted in red. Abbreviations: Ut — Utukok River, Ko — Kokolik River, Ku — Kukpowruk River, Co — Colville River. Also shown is the previously interpreted maximum ice extent for the Pleistocene and Late Wisconsin (LGM) glaciations (Manley and Kaufman, 2002). (For interpretation of the references to color in this figure legend, the reader is referred to the web version of this article.)

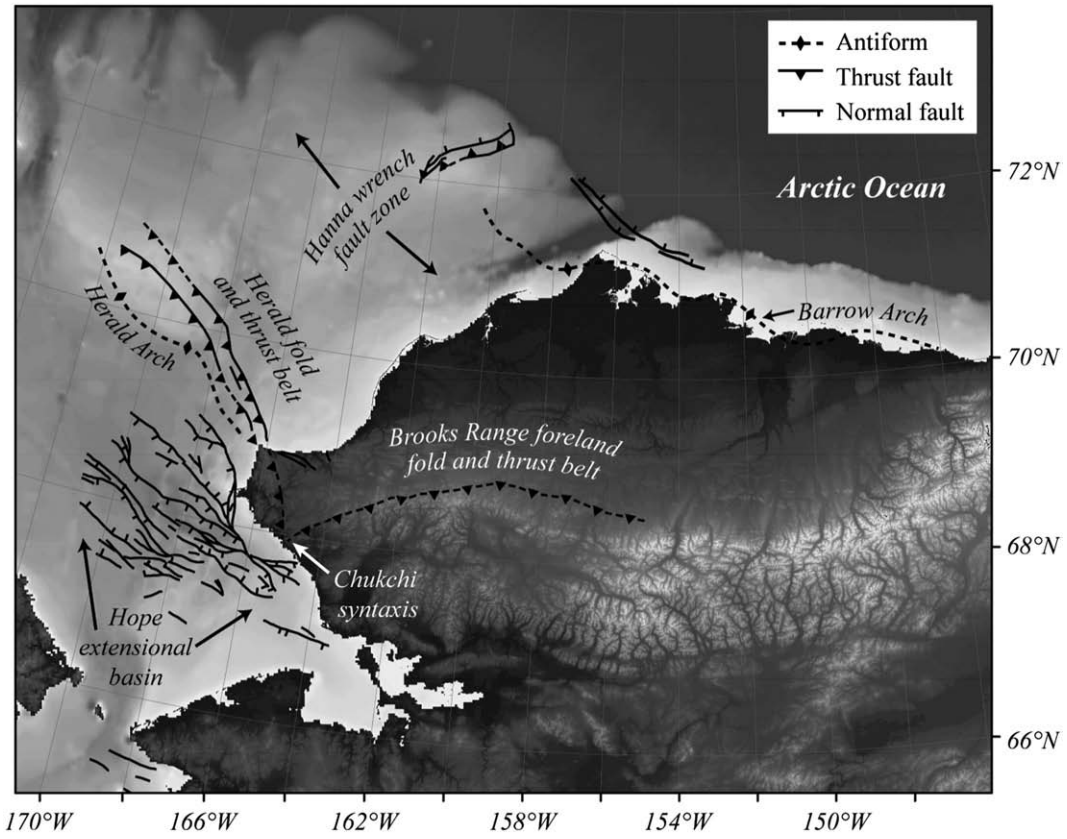

Fig. 2. Simplified tectonic map of northern Alaska and adjacent Chukchi margin with data from Miller et al. (2002).

the thrust belt before emptying into the Beaufort Sea. The few northern rivers that drain west into the Chukchi Sea (e.g., Kukpowruk, Kokolik, and Utukok Rivers) have a combined drainage area of only ~25,000 km^2 (Lamke et al., 1995). The northwestern rivers also have very low discharge, ranging from 500 to 1750 m^3 s^{-1}, compared with a discharge of 6700 m^3 s^{-1} for the Colville River (Childers et al., 1979).

Previous authors have suggested that the primary drainage to the Chukchi Sea during periods of lowered sea level was derived from southwestern Brooks Range and flowed northwest through Hope Valley, emptying into the Arctic Ocean via the Herald Canyon (McManus et al., 1983). While this may be true for the southern Chukchi Sea, the structural high of the Herald Arch effectively prevents drainage from the Hope Basin from reaching the northeastern shelf. Paleochannels linked to rivers in the northernmost part of Alaska appear to trend northward, bypassing the shelf and flowing down Barrow Canyon (Phillips et al., 1988). The small rivers of the northwest Alaska appear to be the sole source of discharge to the region northeast of the Herald Arch.

2.3. Recent glaciations

Controversy exists regarding the extent and volume of glaciation across the western Arctic during the LGM. Several authors have argued that the Beringian landmass remained largely ice-free throughout the LGM, with small glaciers restricted to upland regions (e.g., Brigham-Grette, 2001; Brigham-Grette et al., 2004). The Alaska Paleoglacier Atlas (Manley and Kaufman, 2002) indicates that glaciation was limited to alpine and montane regions during the LGM, while the maximum extent of glaciation is proposed to have occurred during the late Pleistocene, with ice extent mapped to edge of the Brooks Range foothills (Fig. 1). Note the Alaska Paleoglacier Atlas assigns a low level of certainty to the western extent of glacial boundaries, including the northwestern foothills. High certainty boundaries have well-defined chronologies, while low certainty boundaries may encompass areas, such as the northwestern foothills, lacking detailed air photograph or field based studies (Fig. 1). Alternatively, Grosswald and Hughes (2002, 2004) suggest that a large ice shelf extended from eastern Siberia across the western Arctic that would have abutted surrounding continental margins and moved south through the Bering Strait.

Several recent studies have shown evidence for large grounded ice shelves on the Chukchi Borderland and greater Arctic Ocean interpreted to have occurred during older Pleistocene glaciations; however, there is some evidence glacial scours and flutes indicative of ice movement from the shallow Chukchi shelf during the LGM (Polyak et al., 2001; Jakobsson et al., 2005).

3. Methods

CHIRP subbottom data were acquired aboard the USCGC Healy on the Chukchi midshelf (Fig. 1) in 2002, using the Scripps Institution of Oceanography EdgeTech X-Star CHIRP subbottom reflection sonar with sub-meter vertical resolution. Data were acquired at a ship speed of ~4–5 knots. Towfish navigation was obtained by monitoring fish depth and the winch cable payout in relation to topside DGPS receivers. The subbottom reflection profiles were acquired using a 1–6 kHz CHIRP signal with a 50 ms sweep. The CHIRP subbottom data were processed using SIOSEIS (Henkart, 2006) and Seismic Unix (Cohen and Stockwell, 1999) seismic processing software packages. Boomer subbottom data were collected by the U.S. Geological Survey (R. Lawrence Phillips, chief scientist) aboard the *R/V Surveyor* and *R/V Discoverer* in 1984 and 1985, respectively. The USGS Boomer data were collected using an ORE Geopulse subbottom profiler at 100, 150, 175 and 200 J with single channel 25 or 50 element hydrophones. The Boomer subbottom profiles presented here were digitally scanned from paper records. For more information about the USGS expeditions, see Phillips et al. (1988) and Miley and Barnes (1986).

The CHIRP subbottom profiles were used to select piston and vibracore locations across the shelf to construct a relative sea level curve and drainage history for the region. Difficulties with station keeping abilities in sea ice-free conditions limited the number of cores we were able to acquire and in some cases drift in the ship position caused the core locations to be offset from the profiles. The core locations are correlated with the subbottom profiles by projecting the core location orthogonally onto the plane of the subbottom profile and this projection distance is noted in each figure. In order to correlate the cores to the CHIRP profiles, the two-way travel time was converted to depth employing a nominal sound velocity of 1500 m/s. Grain size analyses were performed on selected core sections with a 1 cm sampling interval using a Beckman–Coulter Laser Diffraction Particle Size Analyzer LS13320. Articulated bivalve mollusks and benthic foraminifera samples were collected for ^{14}C dating at the National Ocean Sciences Accelerator Mass Spectrometer (NOSAMS) facility in Woods Hole, Massachusetts. Radiocarbon dates were calibrated to calendar years using the Fairbanks0805 calibration curve (Fairbanks et al., 2005) with a ΔR of 300, corresponding to a ~700 yr reservoir correction. While there appears to be a great deal of variability in reservoir ages across the Arctic, the choice of 700 yr is consistent with other studies from shallow Arctic regions (e.g., Forman and Polyak, 1997; Bondevik et al., 1999; Cook et al., 2005; Keigwin et al., 2006). Variations in the actual reservoir age (±100 yr) may introduce some uncertainty into our age estimates; however, this should not affect the overall conclusions of this paper.

4. Results

4.1. Acoustic facies

4.1.1. Cretaceous strata

The deepest unit imaged on the shelf consists of steeply inclined, folded and faulted strata with a predominantly northward dip. The tilted strata are most prominent in close proximity to the Herald Arch, where they commonly outcrop at the seafloor or have very thin (<1 m), discontinuous sediment cover (Fig. 3). Strata in the north are more acoustically transparent and appear truncated horizontally, with a highly reflective, uneven erosional surface that may have up to 25 m of sediment above. Previous authors interpret this deposit as Cretaceous age strata deformed as a result of thrusting along the Herald front (Phillips et al., 1987, 1988; Thurston and Theiss, 1987).

4.1.2. Southern valley

A large incised valley (~24 km wide) trends along the axis of the Herald Arch for at least ~90 km across the midshelf, downcutting the underlying Cretaceous strata by 50 m (Fig. 4). Subbottom profiles on the landward side of the incised valley suggest that multiple smaller valleys may converge to form the large midshelf valley, which appears to widen and deepen offshore. The valley has a compound fill made up of several distinct depositional units that are defined by six regionally extensive erosional surfaces. In many cases, these erosional surfaces appear to coalesce along the boundaries of the incised valley.

The deepest incision, Valley Incision 0 (VI-0), truncates underlying Cretaceous strata and defines northeastern limit of the incised valley (Figs. 5–7). The sediment above this reflector (Unit 0) appears acoustically transparent in the CHIRP subbottom data, but displays some inclined bedding with cross-cutting relationships farther offshore in the Boomer subbottom data. Unit 0 deposits are observed only on the NE side of the incised valley (Figs. 5–7). Most of the Unit 0 strata appear to be truncated or removed by incision along a second erosional surface, Valley Incision I (VI-1) (Fig. 8). Strata overlying VI-1 (Unit 1) mostly consists of acoustically laminated, low reflectivity unit that is continuous over long distances and drapes the underlying topography (Figs. 5–7). Some internal truncation of reflectors and small channels are present within the unit on the most landward subbottom profiles (Figs. 5 and 6).

Erosion by Valley Incision II (VI-2) truncates and downcuts Unit 1 strata across most of the valley (Figs. 5–7). Incision along VI-2 appears to deepen offshore. The most nearshore profiles show maximum incision of ~15 m, which increases to ~40 m farther offshore. Infill above VI-2 (Unit 2) exhibits a very complex stratigraphy that displays characteristic fluvial cut and fill geometry made up of numerous cross-cutting channels with inferred point bars, cutbanks and lateral accreting sets. Individual channels in Unit 2 are several hundred meters wide with 10–15 m of incision (Figs. 5 and 6).

The two most recent incisions, Incision III (I-3) and Incision IV (I-4), downcut into Unit 2 strata. I-3 has a maximum incision of ~45 m into Unit 2 strata, while I-4 downcuts at least 20 m within I-3 (Fig. 6) and the incision deepens offshore. The two incision surfaces are

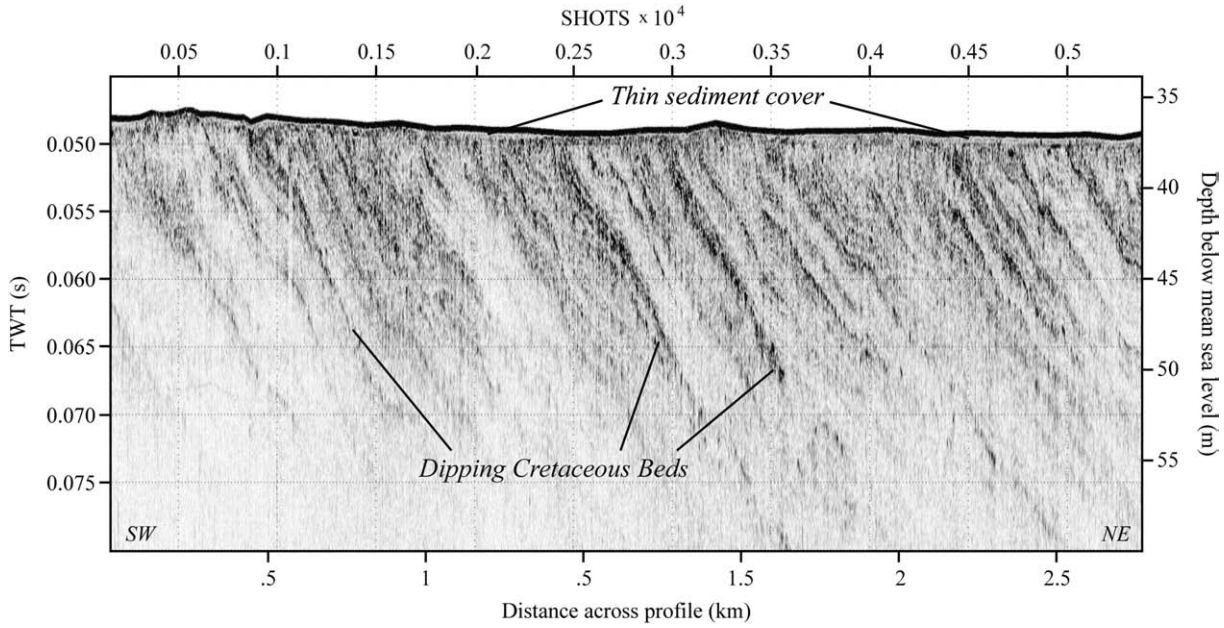

Fig. 3. CHIRP subbottom profile (see Fig. 1 for location) showing northward dipping Cretaceous strata.

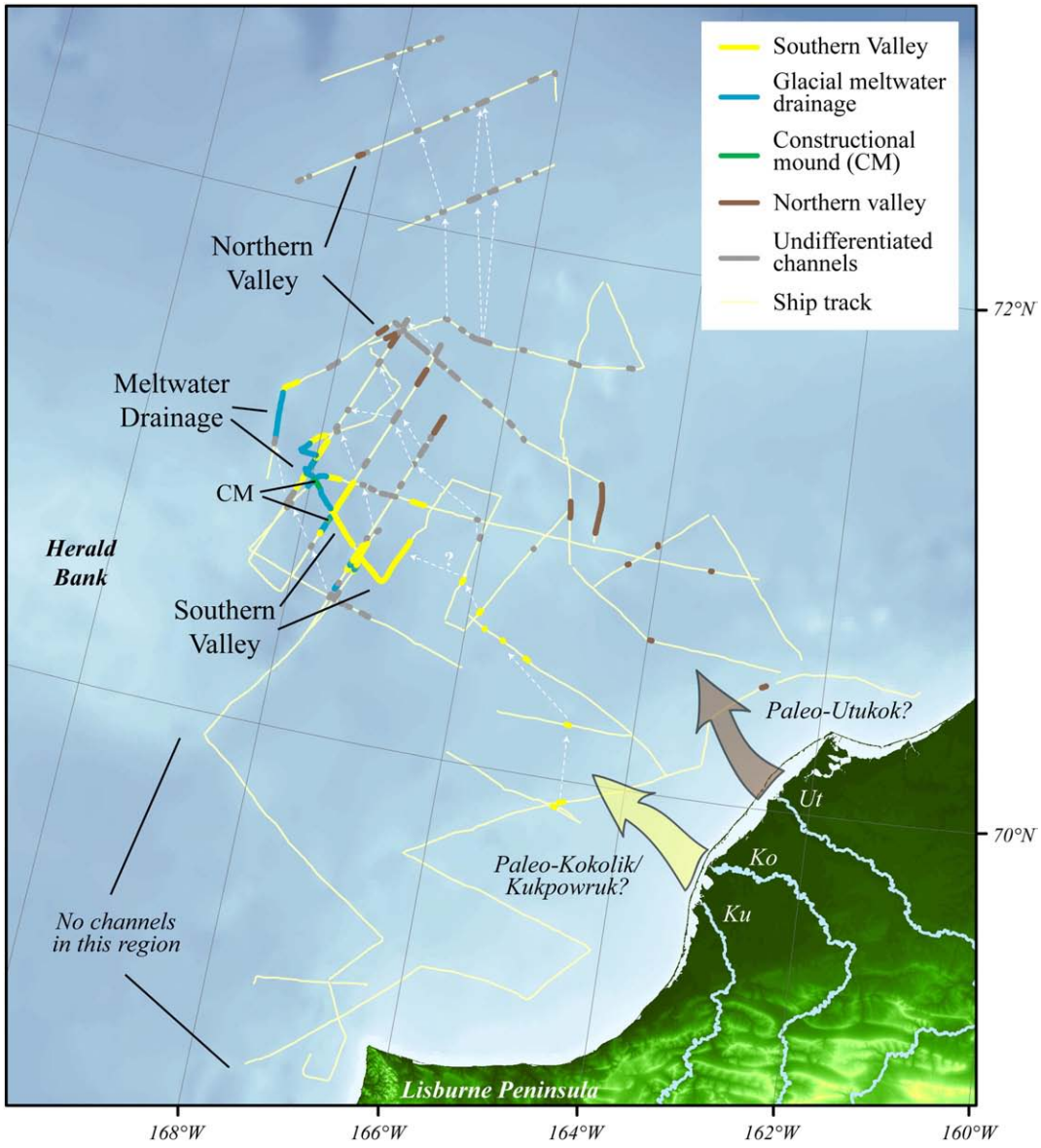

Fig. 4. Interpreted channel map showing profiles crossing the southern incised valley (VI-0, VI-1, VI-2), meltwater drainage (I-3, I-4), constructional mound feature and northern valley. Numerous additional individual paleochannels are also identified in profiles across the shelf; however lack of stratigraphic overlap makes it difficult to definitively correlate these units. Tentative correlations between these smaller channels and valleys are shown.

sometimes difficult to differentiate and may coalesce seaward. Both I-3 and I-4 appear to be restricted to the southwestern side of the incised valley, with widths ranging from 3 km on landward profiles to 15 km seaward (Figs. 4 and 8). The sediments above I-3 (Unit 3) and I-4 (Units 4 and 5) have a very similar acoustically laminated character and are much more reflective than lower units (Figs. 5–8). Unit 3, 4 and 5 strata infill the valley with slight thickening observed toward the basin depocenter. In some profiles, the contact between Unit 4 and Unit 2 is characterized by a relatively rough erosional surface (Fig. 6). In addition, there is some small, localized post-depositional faulting in Unit 4 (Figs. 6 and 7). Units 4, 5 and 6 are separated by local flooding surfaces (FS1, FS2) identified most clearly on CHIRP line 2 (Fig. 6).

A large constructional mound (~2 km wide, 15 high) is observed on the southwestern side of the southern incised valley, situated above Units 1 and 2 (CM; Figs. 5–8). The feature is adjacent to I-3/I-4 and onlapped by strata within Unit 4. Sediment within the constructional mound exhibits downlapping along two surfaces. The upper internal downlap surface occurs roughly mid-section, while the lower downlap surface defines the contact between the constructional mound and the underlying sediment (Figs. 5 and 6). The uppermost reflectors on the NE side of the feature show minor truncation by I-3/I-4 and the feature is onlapped by Unit 3 and/or 4 (Figs. 5 and 6). The constructional mound is present in multiple subbottom profiles, including an orthogonal crossing of two Boomer subbottom profiles that provides evidence of a three dimensional structure (Fig. 8).

4.1.3. Northern valley

Another heavily channelized region is observed on the northern Chukchi midshelf. Compared with the incised valley to the south, drainage in this area appears to less confined, with multiple individual channels and valleys cut into the Cretaceous strata (Figs. 4 and 9). The largest valley in the region, termed the northern valley, downcuts and incises the Cretaceous strata by ~35 m, with widths ranging from 5 to 8 km (Fig. 9). Unlike the incised valley to the south, the northern valley only exhibits one acoustic fill, Unit N1. Unit N1 is acoustically laminated with low reflectivity, an acoustic character similar to Unit 1 observed in the southern valley. There is a ~15 m thick inclined wedge of sediment at the base of N1 on the SW edge. The overlying strata onlap this wedge

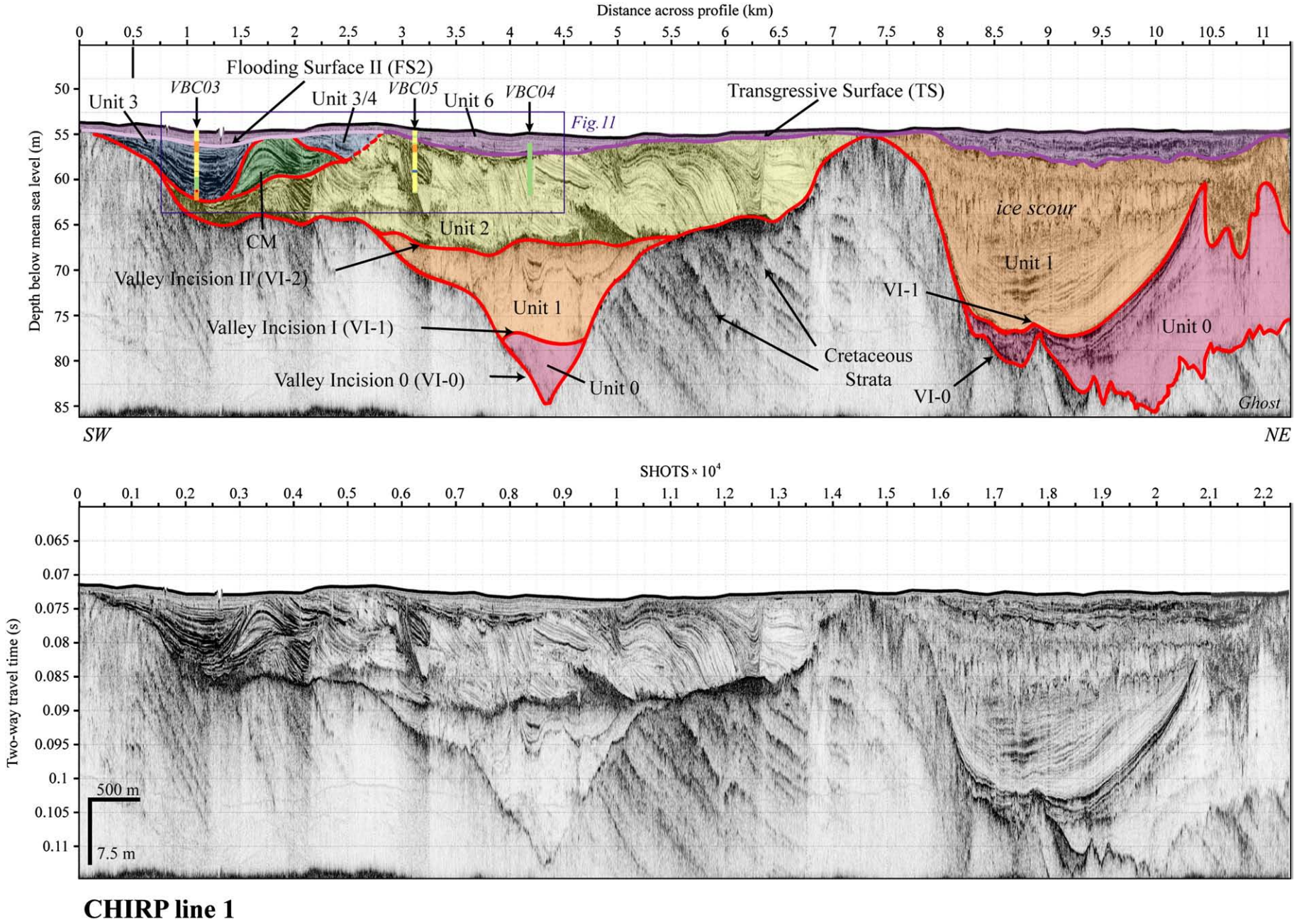

Fig. 5. CHIRP subbottom profile across the incised valley (line 1). Bottom: Uninterpreted profile. Top: Interpreted profile with the reflectors color coded as follows: Red — Valley Incisions 0, 1, 2 (VI-0, VI-1, VI-2); Dark purple — Most recent transgressive surface (TS); Light purple — Flooding surface (FS2). Sedimentary units are also labeled. (For interpretation of the references to color in this figure legend, the reader is referred to the web version of this article.)

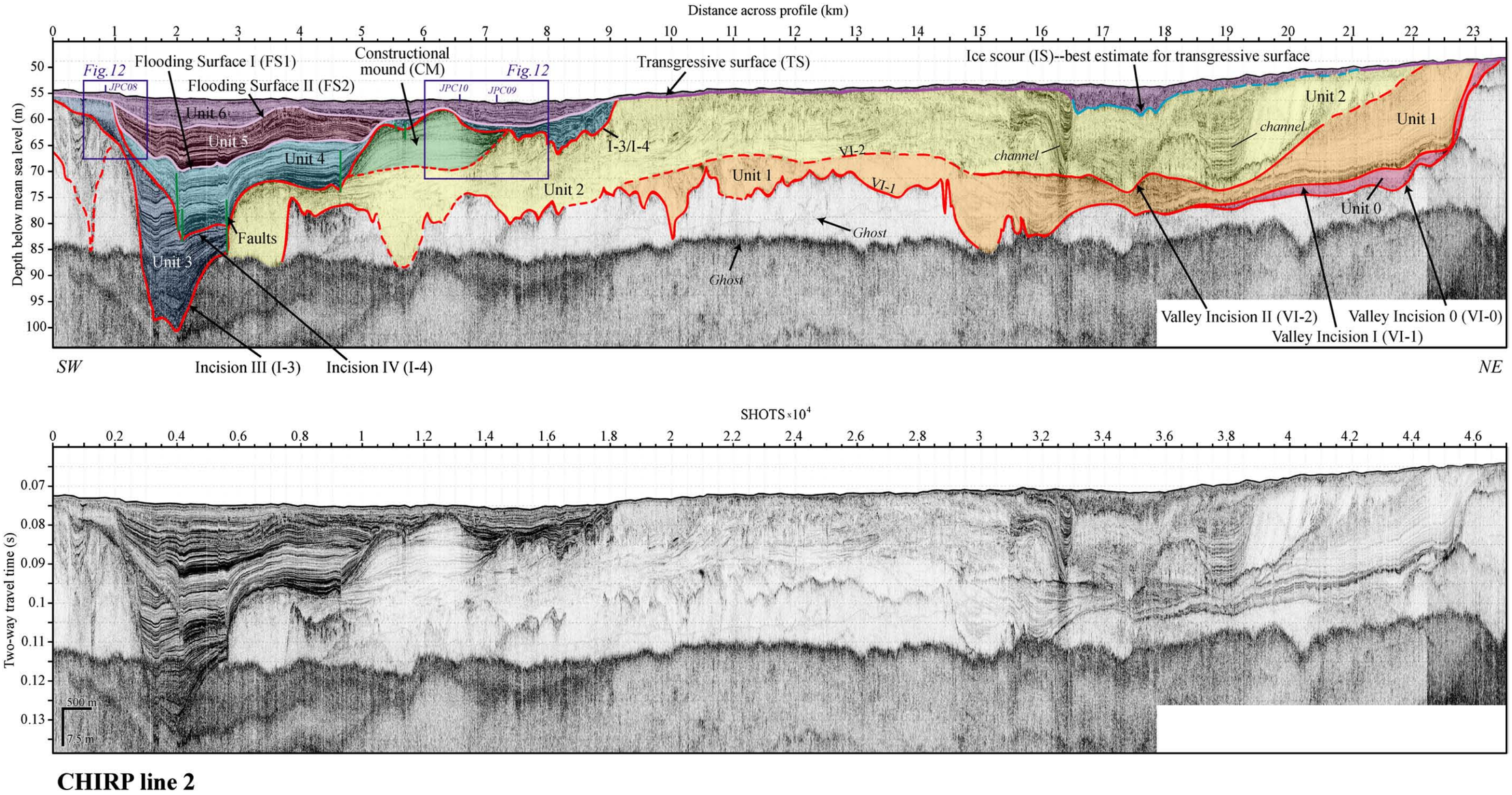

Fig. 6. CHIRP subbottom profile across the incised valley (line 2). Bottom: Uninterpreted profile. Top: Interpreted profile with the reflectors color coded as follows: Red — Valley Incision I (VI-1), Valley Incision II (VI-2), Incision III (I-3) and Incision IV (I-4); Light purple — Flooding surfaces (FS1, FS2); Dark purple — Most recent transgressive surface (TS); Blue — Most recent ice scour (IS), also the best estimate for TS in that area; Green — Post-depositional faulting. CM indicates a constructional mound feature. Sedimentary units are also labeled and core locations of JPC 08, 09, 10 are shown. (For interpretation of the references to color in this figure legend, the reader is referred to the web version of this article.)

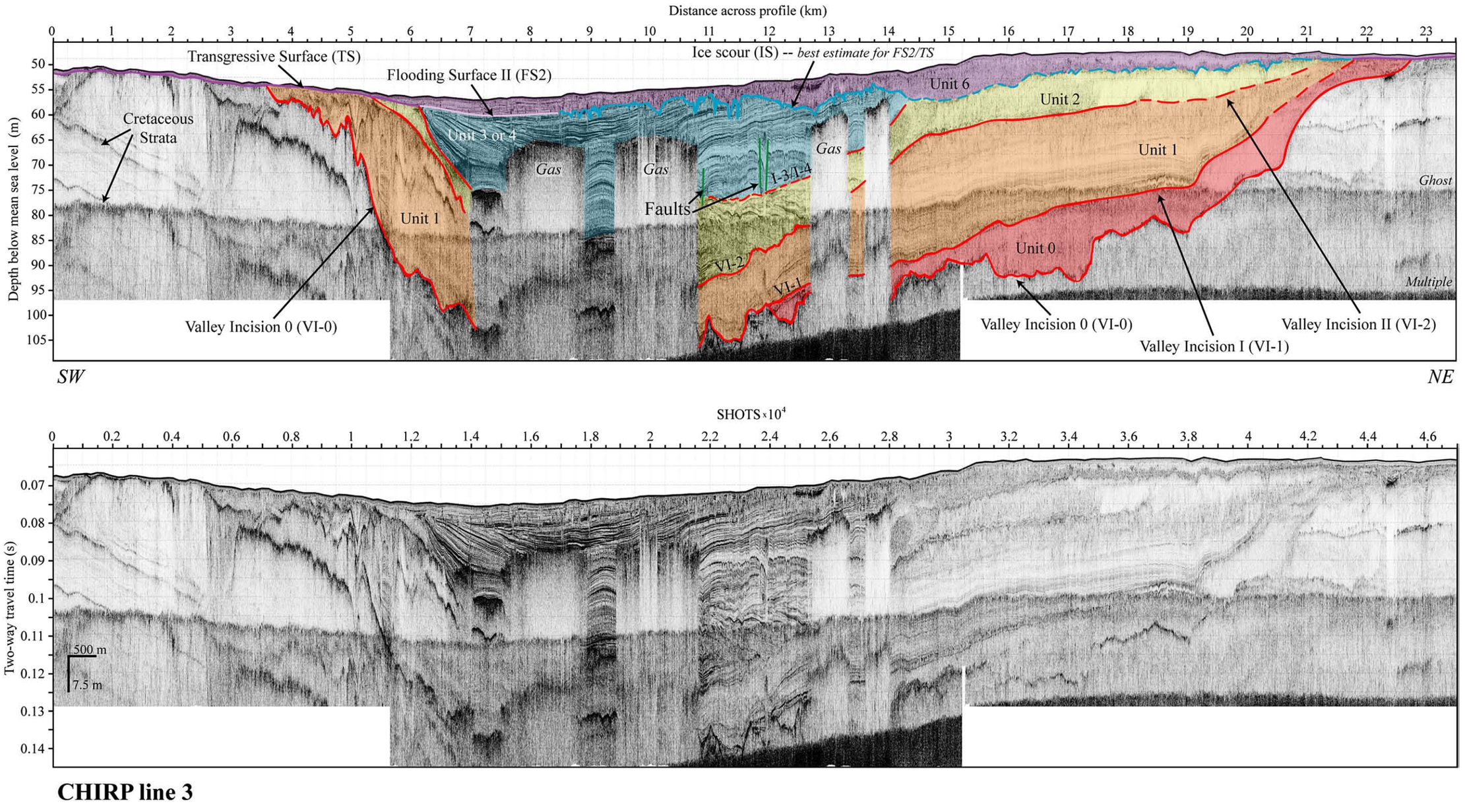

Fig. 7. CHIRP subbottom profile across the incised valley (line 3). Bottom: Uninterpreted profile. Top: Interpreted profile with the reflectors color coded as follows : Red — Valley Incision I (VI-1), Valley Incision II (VI-2), Incision III (I-3) and Incision IV (I-4); Light purple — Flooding surface (FS); Dark purple — Most recent transgressive surface (TS); Blue — Most recent ice scour (IS), also the best estimate for TS in that area. Gas in the shallow sediment results in acoustic wipeouts that obscure deeper reflectors. (For interpretation of the references to color in this figure legend, the reader is referred to the web version of this article.)

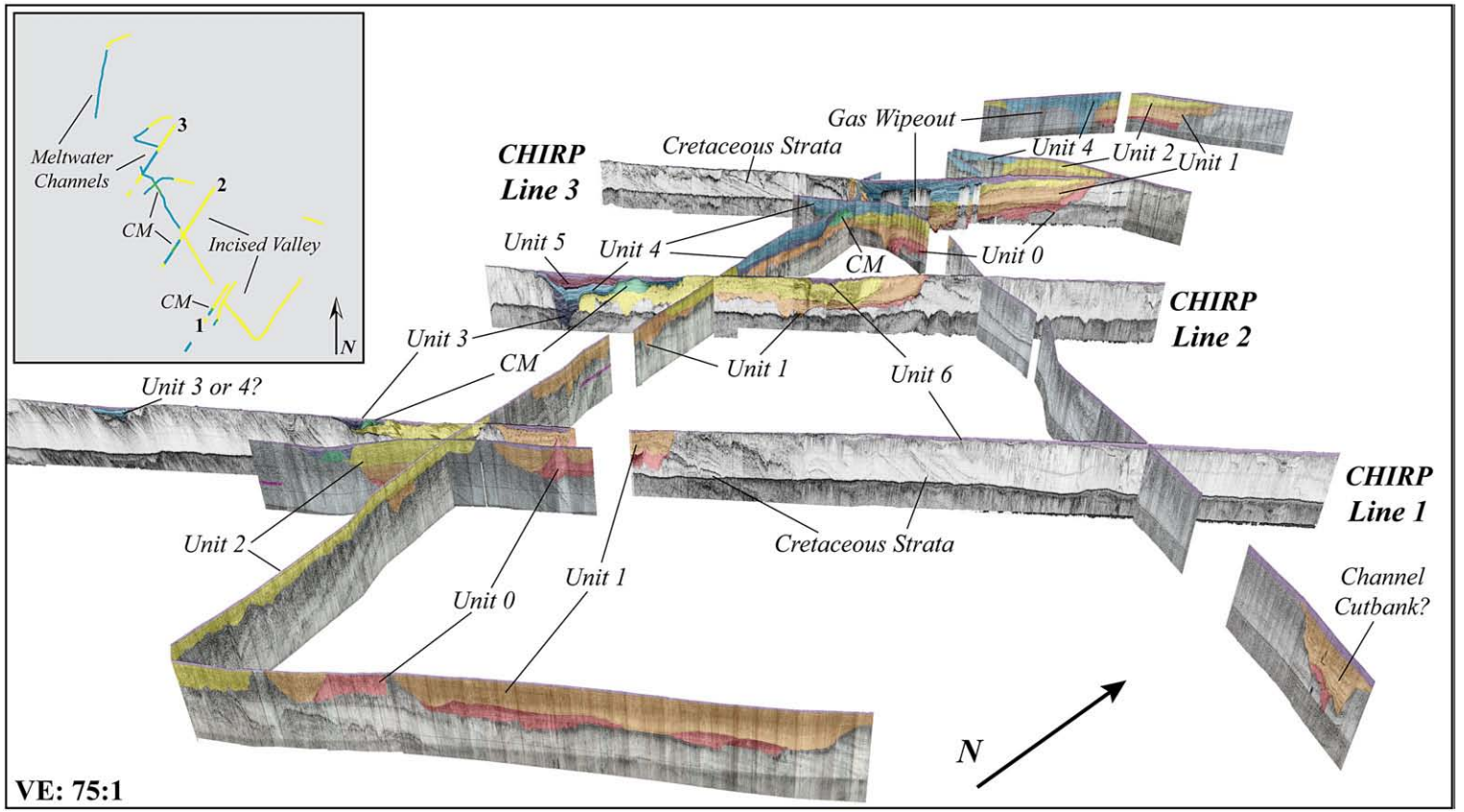

Fig. 8. 3-D perspective view of CHIRP and boomer subbottom profiles across the incised valley region, looking offshore. There is a strong correlation of units across the valley. The incised valley is continuous across 90 km on the shelf and is cut into steeply dipping, folded and faulted Cretaceous strata. Inset: Channel map, see Fig. 4 for reference.

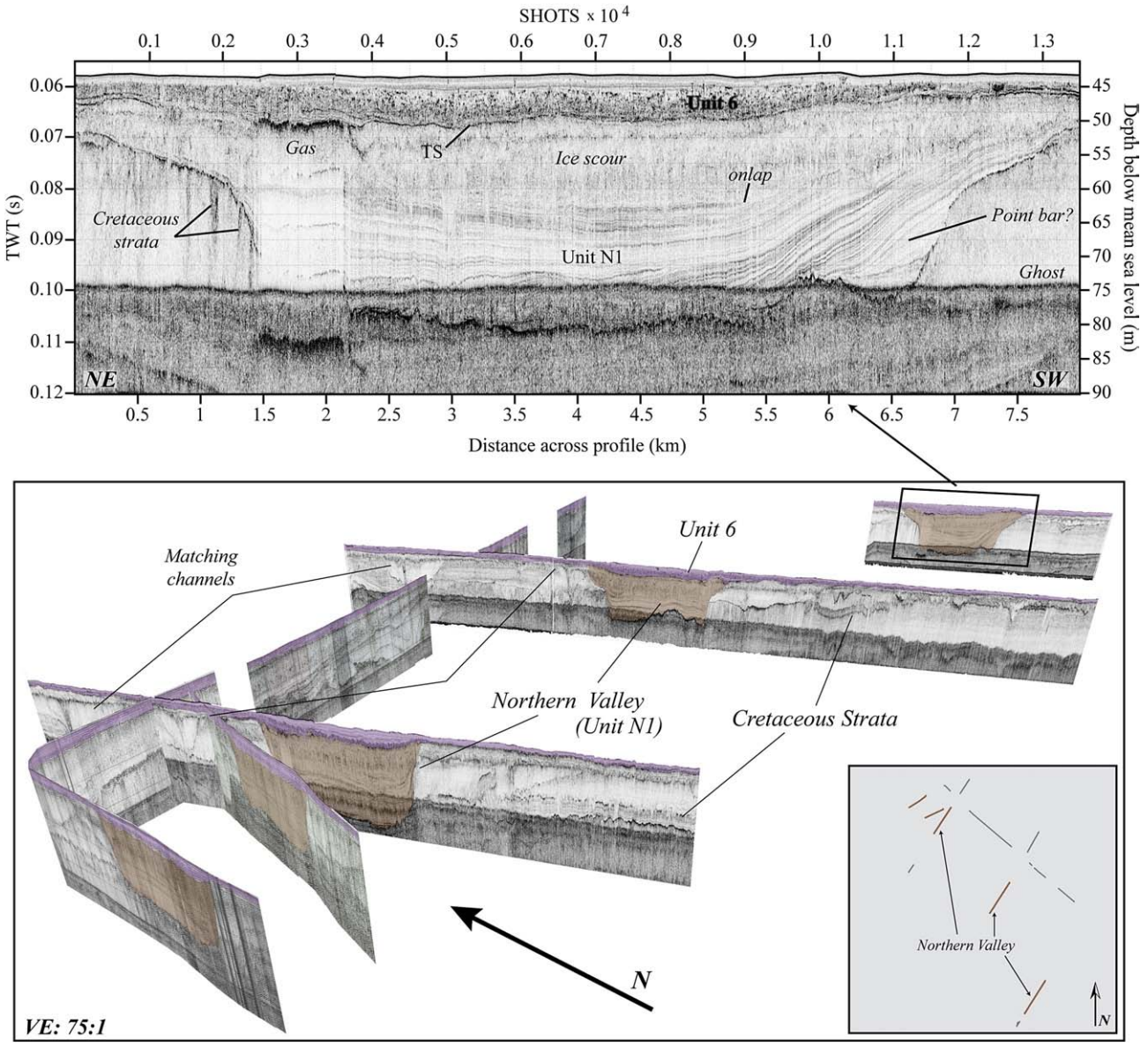

Fig. 9. Bottom: 3-D perspective view of CHIRP and boomer subbottom profiles across the northern valley region, looking onshore. In addition to the large northern channel (shown in brown), several other channels can be correlated. Inset: Channel map, see Fig. 3 for reference. Top: CHIRP subbottom profile across the northern valley. Possible fluvial fill in the base of the valley grades upward to marine sediment that onlaps the underlying topography. The valley is overlain by marine sediment of unit 6, observed across the shelf. (For interpretation of the references to color in this figure legend, the reader is referred to the web version of this article.)

and infill the valley. Reflectors in the upper few meters of N1 sediment appear somewhat chaotic and are disrupted by abundant small v-shaped incisions. Several smaller channels and valleys are present surrounding the northern valley (Figs. 4 and 9); however, given the diffuse drainage and lack of stratigraphic overlap, it is difficult to trace regional surfaces across the valleys or distinguish individual depositional units outside of N1.

4.1.4. Incision of small channels and valleys

Numerous individual paleochannels and small valleys (1–2 km width) are observed across the Chukchi shelf from the most nearshore subbottom profiles out to at least ~55 m water depth (Fig. 4). Incision depths in the channel thalwegs range from 10 to 35 m. The maximum depth of channel base with respect to modern sea level averages ~55 m in the nearshore region, whereas the depth to the channel thalweg is 85–100 m below modern sea level in the northern and southern valleys (Fig. 10). Note there is a marked change in channel depth at approximately 175 km from the coastline, between the paleo-Kokolik/Kukpowruk and the southern valley and the paleo-Utukok and the northern valley. The large profile spacing and lack of stratigraphic overlap makes it difficult to draw any conclusions about relative ages or depositional units between the southern and northern channel systems. There appear to be two drainage pathways emanating from the northwestern Alaskan margin. One series of paleochannels appears to link the Kokolik and/or Kukpowruk Rivers with the southern valley, while the other may link the Utukok River with the northern valley (Fig. 4).

4.1.5. Regional transgressive surface

The uppermost erosional surface (TS) observed in the subbottom profiles truncates strata along the boundaries of both the northern and southern valleys as well the surrounding shelf (Figs. 5–9). In some areas reflector TS is interrupted by small, discrete, v-shaped downcutting events on the NE side of the southern incised valley (IS; Figs. 6 and 7). The sediments above TS (Unit 6) are acoustically laminated

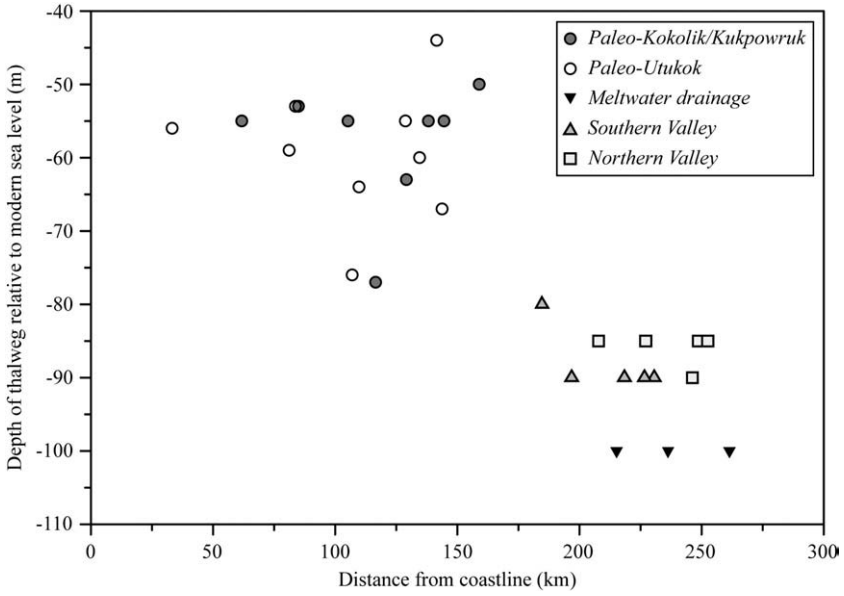

Fig. 10. Plot showing the base of paleochannel (or valley) thalwegs relative to modern sea level versus distance from the coastline.

with low reflectivity. Unit 6 infills bathymetric lows and exhibits thickness variations ranging from <1 m on the interfluves to >5 m in some of the paleochannels (Fig. 8). The transgressive surface in portions of the southern valley separates Unit 6 from the older underlying Units 1 and 2 (Figs. 5 and 6). Along the southern edge of the valley, TS coalesces with I-3 (Figs. 5 and 6).

4.2. Sediment facies

4.2.1. Southern valley

Six sediment cores were collected within the southern incised valley and correlated with the subbottom data. While is some uncertainties are introduced through the projection of core locations onto the plane of the subbottom profiles, two of the key cores from which radiocarbon dates were obtained (VBC03 and JPC10) were collected sediment a very short distance (~15 m) away from the subbottom tracklines. The other cores appear to have collected regionally extensive horizons such that the presented correlation is appropriate.

VBC03 (8.66 m) recovered sediment from Units 3 and 6 on the southwestern side of the southern incised valley (Figs. 5 and 11). The base of VBC03, just above I-3, consists of well-sorted medium sand above interbedded sand and silt. This section contains some of the coarsest sediment collected across the shelf. In addition, there is a large (~3 cm diameter) mudclast in the basal section, which is coincident with an articulated bivalve mollusk, identified as *Portlandia arctica* (Fig. 11). Radiocarbon dating of this shell yielded an age of 12,300±65 ^{14}C yr BP (~13,500 cal. yr BP). The upper portion of Unit 3 is composed of a several meter thick section of silt with occasional sand layers. Upsection, interbedded sand and silt delineates the contact between Unit 3 and Unit 6. The uppermost section of Unit 6 is a silty clay with abundant shell, wood and charcoal fragments.

VBC04 (5.82 m) and VBC05 (6.94 m) both sampled sections of Unit 2 from the center of the southern valley (Fig. 11). VBC05 also has a cap of Unit 6 silt at the surface, while the upper section (presumably Unit 6) of VBC04 was not recovered due to coring difficulties. Unit 2 sediment from VBC05 primarily consists of silty clay, but also contains a several meter thick section of interbedded sand and silt in the upper section and a thin layer of small clay rip-up clasts mid-core, as well as a layer of fine sand at the base. A thin layer of fine, blocky sand marks the TS surface between Unit 2 and Unit 6 in VBC05. In contrast, VBC04 consists entirely of well-sorted fine sand with a slight downcore coarsening. Neither VBC05 nor VBC04 recovered any biogenic material.

JPC08 (3.67 m) recovered sediment from Units 3 and 6 (Fig. 12). The upper ~1 m of JPC08 consists of silty, shell rich clay from Unit 6. Just beneath Unit 6, Unit 3 contains interbedded fine sand and silt that grades downward into visually homogenous silty clay in the basal section, but shows faint laminations on an X-ray image. JPC09 (8.92 m) and JPC10 (8.13 m) both recovered sediment from Units 4 and 6, as well as from the northeastern edge of the constructional mound feature below I-4 (Fig. 12). The base of JPC09 is comprised of fine sand with clay rip-up clasts that are coincident with the contact between the constructional mound feature and Unit 2. Above is a thin layer of interbedded silt and sand overlain by ~2 m of well-sorted medium-fine sand (median grain size ~175 μm) that correlates with the constructional mound feature. Similar to JPC09, the lower section of JPC10 consists of ~4 m of well-sorted sand that also corresponds to the constructional mound feature; however, the JPC10 sand is slightly finer (median grain size ~150 μm) than the sand in JPC09. Clay rip-up clasts (2–10 cm) at the base of JPC10 are coincident with an internal downlap surface in the constructional mound feature. Both cores exhibit a slight fining upward at the top of the sand sections before transitioning to the interbedded sand and silty clay at the interface between the constructional mound feature and Unit 4. JPC09 has a more expanded Unit 4 section than JPC10, characterized by a thin layer of clay rip-up clasts, in between sections of interbedded sand and silt. The upper ~4 m of both cores consists of the silty/sandy clay of Unit 6 with shell fragments. Radiocarbon dates were obtained from articulated bivalve mollusks at several depths within the Unit 6 section of JPC10 (Fig. 12). The ages yield an average sedimentation rate of ~1.45 m/kyr, from 8000–10,700 yr BP, decreasing to ~0.05 m/kyr in the last 8000 yr.

4.2.2. Hope Valley

A piston core (JPC02) in the central Hope Valley recovered a ~9.5 m thick Holocene section (Fig. 13). The base of the core contains interbedded sand and silt that coarsens upward to a 55 cm thick well-sorted sand section, with a slight fining upward. A much finer section of interbedded silt and sand creates an abrupt transition at the top of the sand. This section is overlain by 8.5 m of silt that correlates with Unit 6. Two abundance peaks of the foraminifer, *Elphidium excavata*, yielded radiocarbon dates of 10,900±140 ^{14}C yr BP (~11,900 cal. yr BP) at 845.5 cm, just above the TS transition, and 6920±75 ^{14}C yr BP

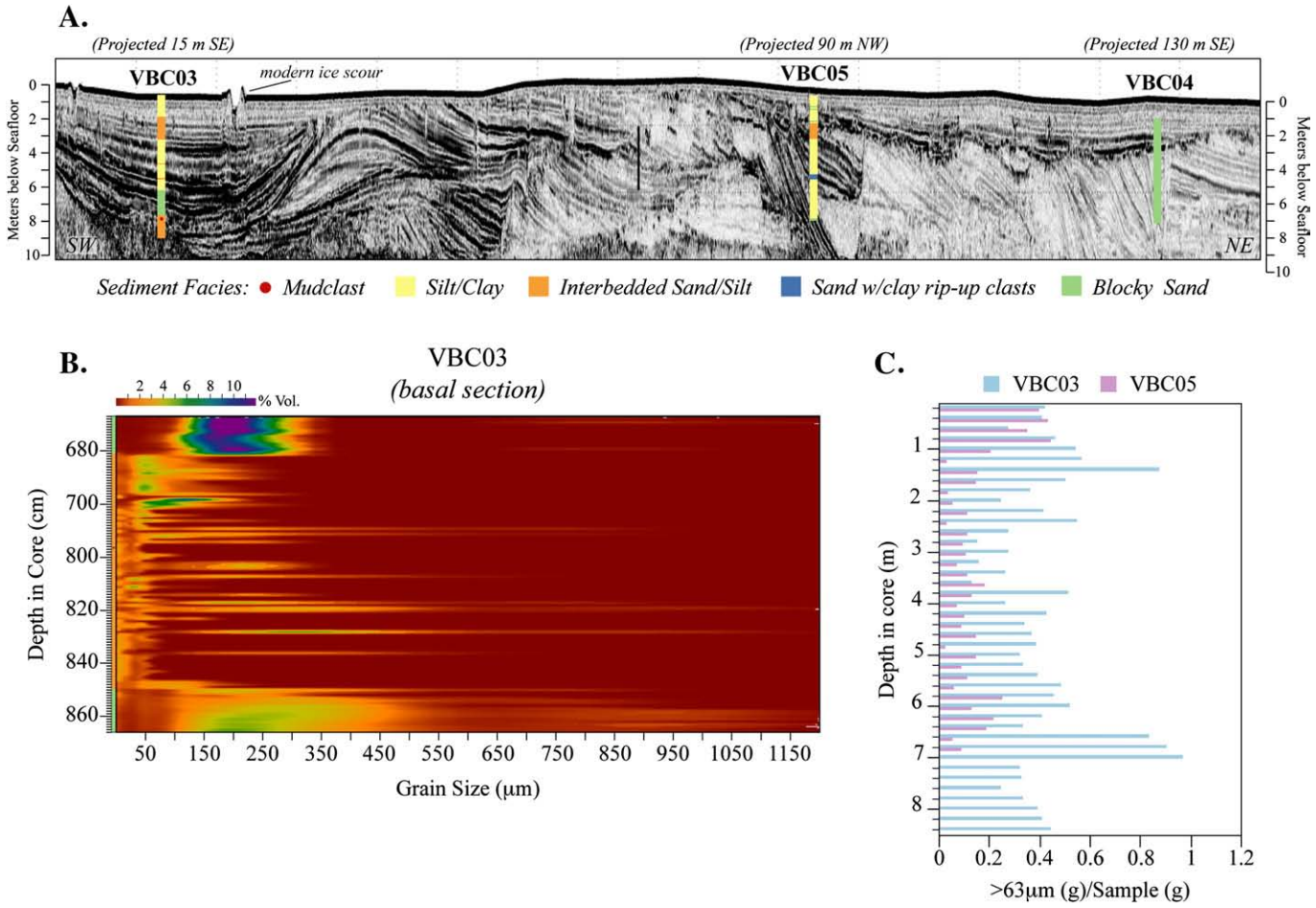

Fig. 11. A. Sediment facies of vibracores in southern incised valley correlated with CHIRP subbottom data. *Articulated bivalve mollusk (12,300±65 ^{14}C yr BP) was recovered from same depth (7.42 m) as the dropstone in VBC03. Note: The upper ~1 m of VBC04 is absent. B. Contour plot of grain size versus depth showing percent volume for 1 cm sampling of the basal section of VBC03. C. Comparison plot of >63 μm size fraction versus depth showing weight percent for 20 cm sampling of VBC03 and VBC05. Note the two cores show similar amounts of coarse fraction in the upper meter, where both cores collected Unit 6 sediment. Below this level, the grain size distributions diverge as VBC03 recovered Unit 3, while VBC05 recovered Unit 2.

(~7100 cal. yr) at 69.5 cm (Keigwin et al., 2006). X-ray fluorescence (XRF) analysis of the basal section shows a major shift in elemental components (Cu, Fe, Ni, Zn and S) at the transition from sand to silt. Keigwin et al. (2006) also report a large increase in δ^{18}O, along with a decrease in δ^{13}C, at this same level.

4.2.3. Outer shelf sedimentation

A suite of six cores on the mid to outer shelf (49–62 m water depth) each recovered several meters of Unit 6 sediment (Fig. 14). All of the cores recovered several meters of silty clay above a fine sand or interbedded sand and silt appears to correlate with a flooding surface observed in the CHIRP subbottom profiles (Fig. 14). Grain size analyses were conducted on the basal sections of VBC39 and VBC40. VBC39 (4.4 m) sampled a well-sorted, fine sand (median grain size ~125 μm) at the base, overlain by an interbedded sand and silt. VBC40 (3.7 m) consists of a bedded, well-sorted fine sand (median grain size ~75 μm) at the base mantled by a unit of interbedded fine and coarse sands, which creates a sharp contact with the basal sands. Overlying the interbedded fine and coarse sands is a silty clay unit in the uppermost section (Fig. 14).

4.3. Onshore drainage

Drainage in northern Alaska is in large part structurally controlled by the Brooks Range. The Colville River appears to have captured most of the northern foothill drainage along the axis of the foreland basin. A low lying drainage divide (~10 m high) near the headwaters of the Colville separates the headwaters for the Utukok, Kukpowruk and Kokolik rivers, which flow westward into the Chukchi Sea (Fig. 15). The northwestern rivers have much lower discharge and smaller combined drainage area than the Colville River, yet appear to be more deeply incised. The headwaters of the northwestern rivers cut across exposed folds of the foothills to form a trellis drainage network. The coastal plain in this region is characterized by numerous thermokarst lakes (Fig. 15C). Both the Utukok and Kokolik Rivers display broad floodplains characteristic of low gradient, meandering rivers. Profiles across portions of these rivers on the coastal plain shows floodplain valley widths of 1–3 km (Fig. 15A). The active flow occupies a small channel surrounded by meander cutoffs and oxbow lakes while the remaining floodplain is heavily sedimented with fluvial deposits. The Kukpowruk River is the most deeply incised of the three, but also has the narrowest valley (~1 km width; Fig. 15A). The Kukpowruk River is also much less sinuous and may have a structural barrier on the eastern side (Fig. 15D).

5. Discussion

5.1. Multiple sea level cycles

The southern incised valley contains three regional erosional surfaces that appear to represent fluvial downcutting during multiple sea level lowering events. Each of these incision surfaces defines a

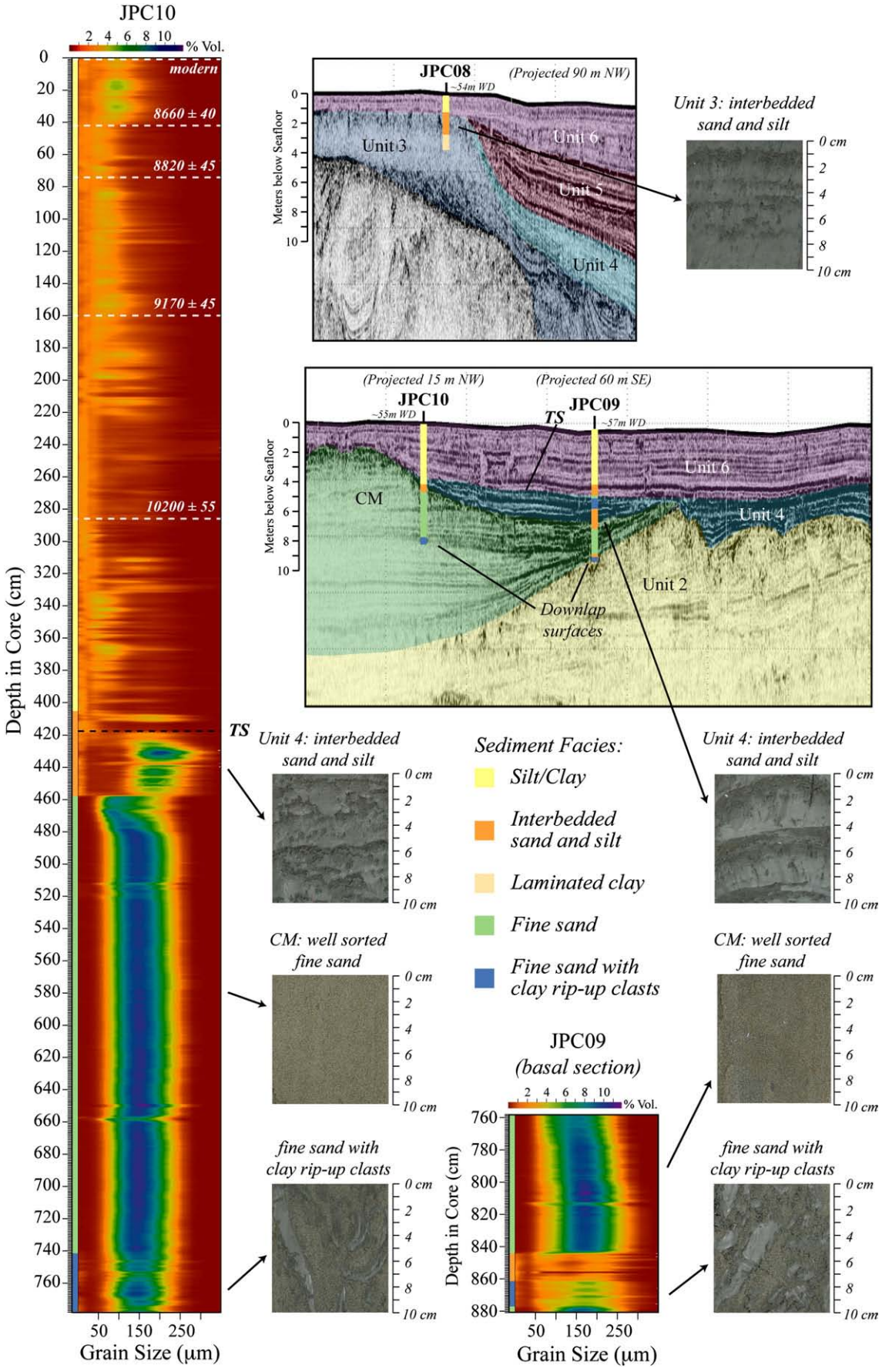

Fig. 12. Sedimentary facies of piston cores in southern incised valley correlated with CHIRP subbottom data. WD = water depth. Contour plots of grain size versus depth showing percent volume for 1 cm sampling analysis are shown for JPC 10 and the basal section of JPC09. Radiocarbon dates from articulated bivalve mollusks in JPC10 are shown on the grain size plot.

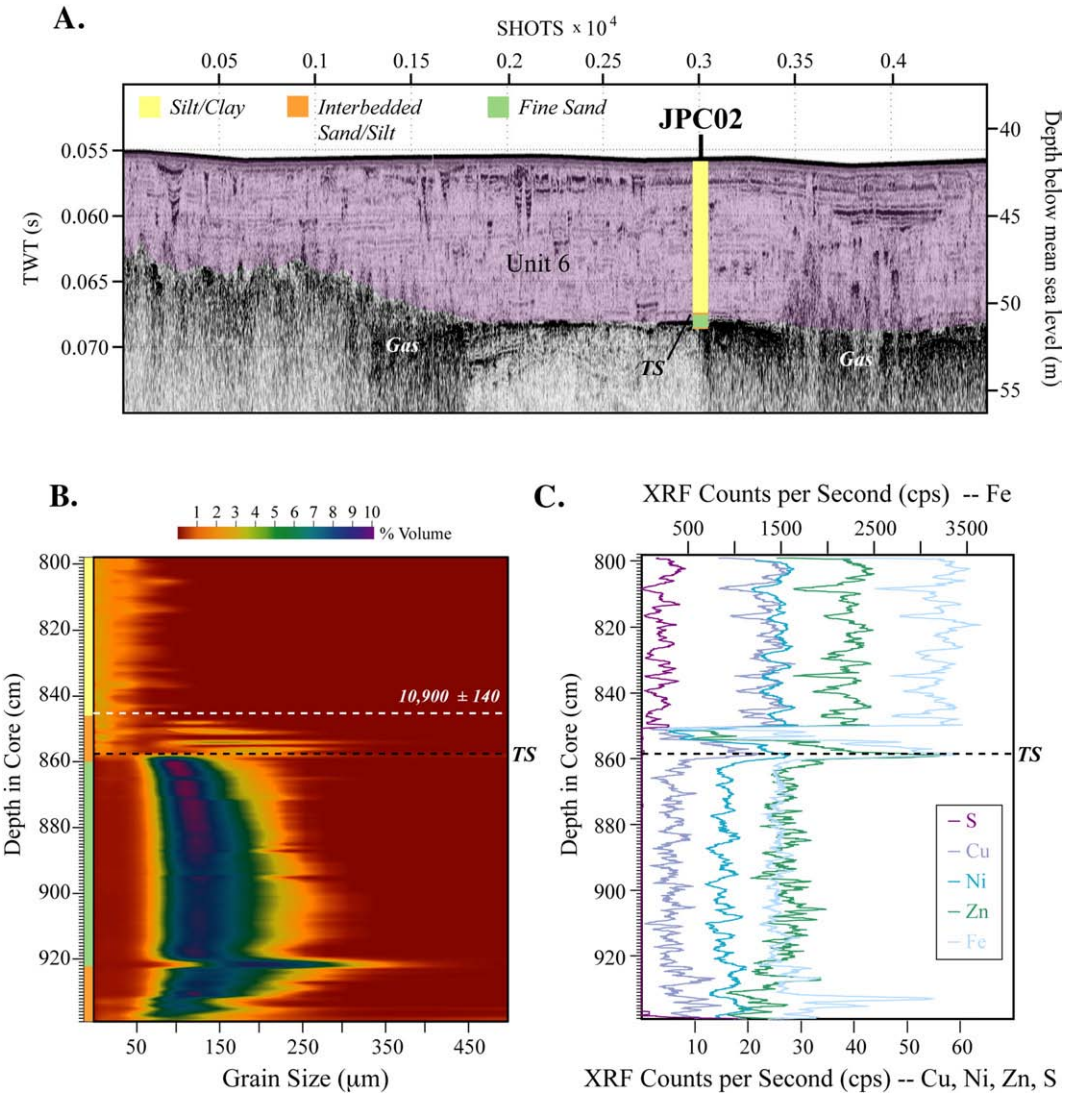

Fig. 13. A. Sedimentary facies of piston core JPC02 in Hope Valley, correlated with CHIRP subbottom data (line 10). B. Contour plot of grain size versus depth showing percent volume for 1 cm sampling analysis of basal section. C. X-ray fluorescence (XRF) analysis for basal section showing counts of Cu, Ni, Zn, S and Fe.

sequence boundary underlying a succession of lowstand systems tract deposits (LST) followed by transgressive systems tract deposits (TST).

In classic sequence stratigraphic incised valley fill models (e.g. Vail 1987; Van Wagoner et al., 1990; Zaitlin et al., 1994), the valley undergoes net fluvial erosion and sediment bypass during the relative sea level fall. During the late part of the lowstand, as the rate of relative sea level fall slows and the rise begins, the valley is filled with backstepping fluvial deposits of the LST, assuming there is sufficient sediment supply. As the valley is flooded, estuarine and open marine deposits of the TST downlap onto the underlying fluvial strata. Typically the TST would be overlain by deposits of the highstand systems tract (HST); however, we do not commonly observe HST deposits across the southern valley region due to a combination of processes. Within the valley, multiple fluvial incisions have reworked and removed any highstand deposits, while on the interfluves highstand deposits are reworked with each transgression due to the limited accommodation space.

The deepest surface, VI-0 (~50 mbsf), represents the oldest phase of incision into the underlying Cretaceous strata. While the acoustically transparent character of Unit 0 in the CHIRP data is difficult to classify, Boomer subbottom profiles across Unit 0 farther offshore exhibit well-defined, inclined beds that may represent fluvial deposition. The majority of Unit 0 has been eroded during a second period of sea level lowering that corresponds to incision along VI-1. Unit 1 contains small channels on CHIRP line 1 (Fig. 5) and some inclined beds in the basal part of the unit along CHIRP line 2 (Fig. 6). The majority of Unit 1, though, contains parallel, draping strata that appear more representative of quiescent deposition. Both Units 0 and 1 appear to represent the classic succession of fluvial deposition within the LST as sea level begins to rise, transitioning upward to estuarine and marine deposition within the TST, creating a drowned valley estuary at the seaward end of the system. The transition form fluvial to marine is predominantly concordant in the incised channels as sediments are infilling the lows and there is little to no erosion across the transgressive surface.

A third phase of sea level lowering is represented by regional erosional surface VI-2 that downcuts and truncates Unit 1 strata. The fluvial strata that make up the majority of Unit 2 appear to record lateral channel migration within the valley. On CHIRP lines 1 and 2 (Figs. 5 and 6), several individual channels can be identified within the deposit that exhibit characteristic fluvial features (e.g., point bars and cutbanks). The upper part of these channels is filled with acoustically laminated sediment that may represent meander cutoff deposits or localized backfilling with marine sediment during the sea level rise. Cut and fill channel architecture is far more common in Unit 2 than Units 0 or 1. Furthermore, there does not appear to be any regionally

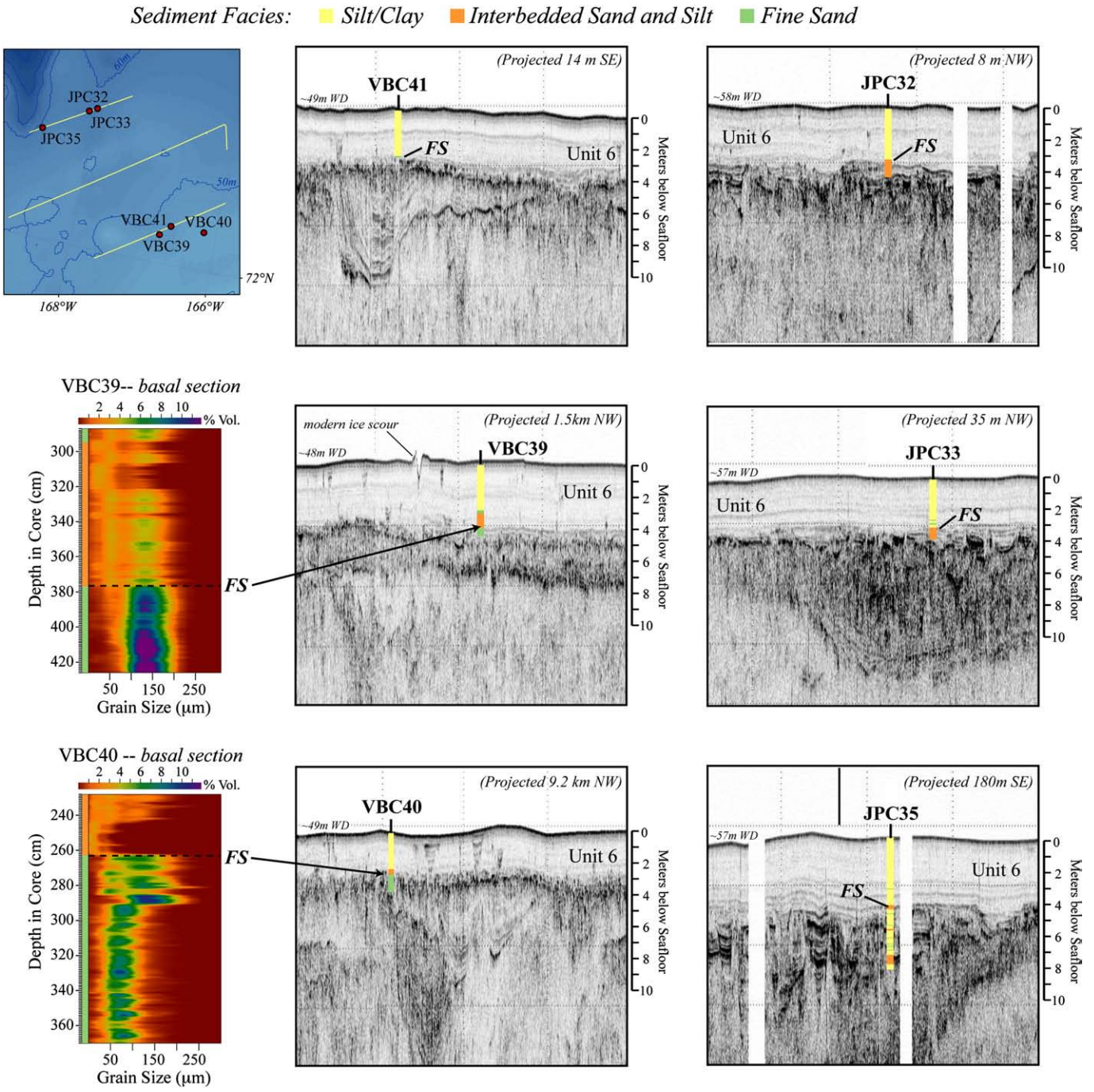

Fig. 14. Sedimentary facies of mid/outer shelf vibracores. WD = water depth. All of these cores exhibit a prominent flooding surface (FS) that is marked by a shift from sand or interbedded sand/silt to silt. Contour plots of grain size versus depth showing percent volume for 1 cm sampling analysis are shown for the basal sections of VBC39 and VBC40. The core positions have been projected onto the profiles as noted.

extensive laminated sequences within Unit 2 as observed in Unit 1. One possible explanation is that rate of sedimentation during this interval may have been high enough to outpace the rate of sea level rise. In such a scenario, nearly the entire valley would be filled with fluvial deposits leaving little accommodation for marine deposits.

The uppermost surface, TS, which truncates strata across both the edges of the northern and southern valleys as well as the surrounding shelf, is interpreted to be a regional trangressive surface. On some subbottom profiles within the southern incised valley, reflector TS is disrupted by numerous v-shaped incisions (IS), indicative of sea ice scouring following the transgression, that obscure the exact location of TS. In these instances, reflector IS is taken as the best estimate for the transgressive surface. TS is overlain by marine strata of Unit 6, which represents post-transgressive Holocene sedimentation associated with the TST. In the southern valley, the TS surface identified in the CHIRP data correlates to a shift from sand or interbedded silt and sand to more homogeneous silt and clay (Figs. 11 and 12). JPC02 in the Hope Valley exhibits similar change in grain size and XRF analyses of the basal section shows a concomitant shift in elemental composition at the grain size boundary. Keigwin et al. (2006) also report a shift in $\delta^{18}O$ that is indicative of a switch from estuarine to open marine conditions at this same level. Radiocarbon dating of the TS within the Hope Valley yields an age of 10,900±140 ^{14}C yr BP (~11,900 cal. yr BP). The oldest radiocarbon date from material within Unit 6 of JPC10 yields an age of

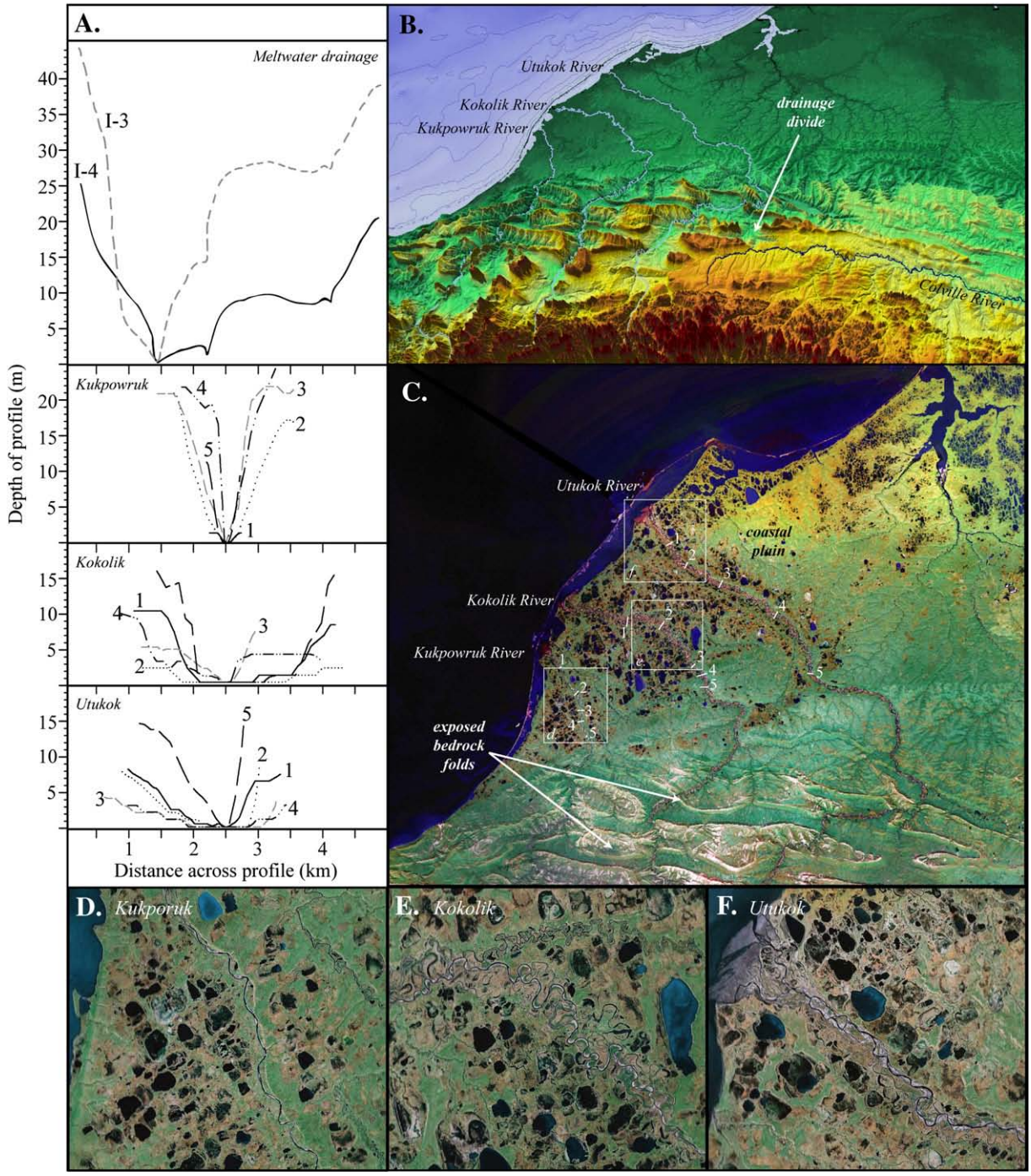

Fig. 15. A. Profiles across the I-3 and I-4 reflectors compared with floodplain profiles across the three dominant northwestern Alaskan rivers inferred to connect with the midshelf valley. The river profiles were measured from a 100 m resolution DEM of northern Alaska (Manley, 2001). B. 3-D perspective view of the topography in northwestern Alaska. The northward flowing trellis drainage incises the east–west trending fold belt of the Brooks Range foothills. C. Satellite imagery of northern Alaska showing river profile locations. D, E, F. Satellite imagery of the northwestern rivers on the coastal plain, showing meandering morphology and broad floodplains within the incised valleys.

10,200±55 ^{14}C yr BP (~10,700 cal. yr BP), approximately 1 m above TS. Using the JPC10 sedimentation rate of ~1.45 m/kyr for this interval to extrapolate the age of TS in both JPC10 and JPC09 yields an age estimate of ~11,500 yr BP, which is consistent with the age of TS within the Hope Valley, and roughly correlates with the timing of the inferred Meltwater Pulse 1-B (Fig. 16).

In general, Unit N1 within the northern valley has a similar acoustic character to Unit 1 in the southern valley. Both deposits exhibit inclined beds at the base that may represent initial fluvial deposition, but are primarily comprised of acoustically laminated strata that are continuous across much of the valley and appear to drape the underlying strata (Figs. 5–9). The dipping strata in both Units 1 and N1 are onlapped by a channel filling sequence that is obscured at the top by multiple ice scouring events. Without stratigraphic overlap between the northern and southern valleys or core information in the northern valley, correlation of these two units is speculative; however, based on acoustic character and these three observed packages (i.e. basal dipping, middle infilling and onlapping, and the upper ice scoured section), we suggest that incision of the northern valley and VI-1 and the overlying fill may record the same sea level cycle.

The exact age of the valley incisions remains unknown; however, several lines of evidence suggest that the features are relatively recent.

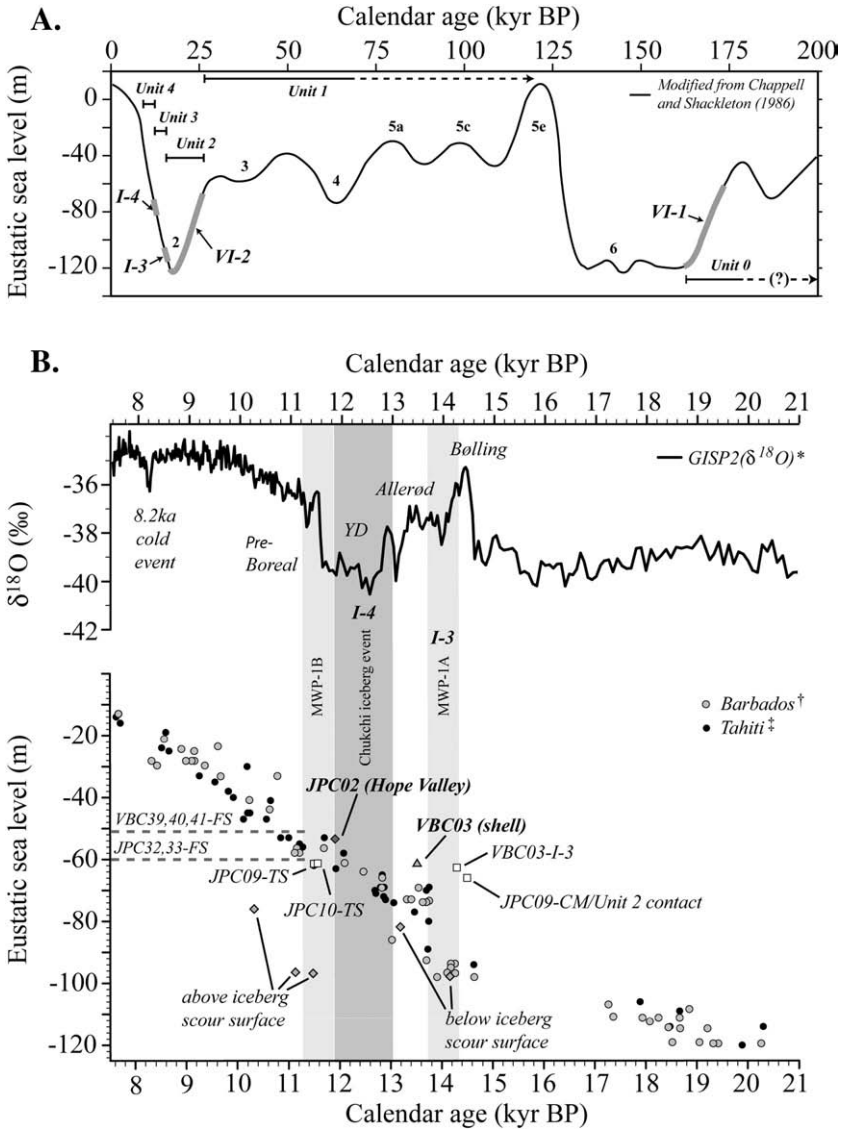

Fig. 16. A. Eustatic sea level curve and associated Marine Isotope Stages (MIS) modified from Chappell and Shackleton (1986). Suggested timing of the incised valley erosional surfaces and seismic facies are shown in relation to eustatic sea level. We interpret VI-2 and VI-1 to correlate with sea level lowering associated with MIS 2 and MIS 6, respectively, while VI-0 must be older. I-3 and I-4 appear to have been downcut during a period of sea level rise following the LGM. B. Climate and sea level records for the last 21 ka. Top: Greenland Ice Sheet Project (GISP) II oxygen isotope record (Stuiver and Grootes, 2000). More positive values indicate warmer temperatures; several climate periods are noted; YD — Younger Dryas. Bottom: Sea level history reconstructed from corals collected in Tahiti (†Bard et al., 1996) and Barbados (‡Fairbanks, 1990) plotted along with new Chukchi data. Dates from JPC02 (Hope Valley FS) and VBC03 (shell), as well as the iceberg scour surface dates are calibrated ^{14}C-based ages. Points from JPC09, JPC10, and VBC03 are extrapolated from ^{14}C dates in JPC10, using the sedimentation rate of 1.5 m/kyr. Diamonds indicate radiocarbon dates from benthic foraminifera; triangles indicate radiocarbon dates from articulated bivalves; squares indicate dates extrapolated using the sedimentation rate from JPC10. Data presented here suggest that incisions I-3 and I-4, which are interpreted to represent meltwater discharge, may correlate with Meltwater Pulse 1-A (MWP 1-A) and the Chukchi iceberg event, respectively. The iceberg scour surface on the outer Chukchi shelf is constrained to between 12,000 and 13,000 cal. yr BP, following a warm period at the onset of the Younger Dryas (Hill and Driscoll, 2006). The regional transgressive surface (TS) appears to correlate with Meltwater Pulse 1-B.

In the southern valley, VI-0 truncates the northward dipping Cretaceous strata. These underlying strata were tilted as a result of thrusting along the Herald Arch, a feature which may have been active as recent as the early Tertiary (Phillips et al., 1988; Moore et al., 1994). The strata within the southern valley are not deformed, suggesting that they must be younger than the age of deformation. The seafloor above the southern valley exhibits ~6 m of negative relief. If the valley was formed in the distant past, we would expect this depression to have since filled with sediment. Additionally radiocarbon dating across the shelf indicates TS is related to the most recent marine transgression (e.g., JPC02, JPC10). Without deep core information from Units 2 and older, the simplest explanation appears to be that the sea level cycles represented by VI-1 and VI-2 correlate to the Illinoian (Marine Isotope Stage 6) and Wisconsinian (Marine Isotope Stage 2) glaciations, respectively (Fig. 16). VI-0 appears to represent an even older phase of sea level lowering, perhaps dating back to Marine Isotope Stage 12. We expect maximum downcutting to have occurred during the period of most rapid sea level lowering, with subsequent deposition of overlying units as sea level began to rise (Fig. 16). By analogy with VI-1, the northern valley may also correlate with MIS 6 and other incisions in the region may be MIS 12 or older.

5.2. Meltwater discharge

Reflectors I-3 and I-4 both exhibit large downcutting relief that truncates underlying Units 1 and 2; however, these two surfaces do not appear to represent sequence boundaries. Units 3 and 4 strata onlap Unit 2, indicating I-3 and I-4, along with the subsequent fill,

must be younger than VI-2 and Unit 2. If VI-2 was indeed incised during MIS 2, I-3 and I-4 must have been downcut during the period of sea level rise following the LGM. Sequence stratigraphic models commonly invoke base level lowering as the primary cause of fluvial incision and downcutting across the shelf; however, climatic factors, such as increased discharge or decreased sediment input, or a combination of both, may generate incision in the absence of relative sea level fall (Schumm et al., 1987; Dalrymple et al., 1994). While sedimentation is generally expected to decrease during the transgression, estimates from both the southern valley (JPC10) and the Hope Valley (JPC02) (Keigwin et al., 2006) indicate that sedimentation rates were relatively high during the most recent transgression and decreased dramatically ~7000 yr BP. In the absence of base level lowering or decreased sedimentation, our preferred interpretation is that the incision resulted from increased discharge in response to meltwater runoff during deglaciation.

Unlike Units 0, 1 and 2, the highly reflective, acoustically laminated sediment of Units 3, 4, and 5 shows no evidence of fluvial structures. VBC03 recovered entirely marine sediment from within Unit 3. The basal section of this core also exhibits relatively coarse grained layers that may represent lag deposits in the base of the channel (Fig. 11B). Therefore we interpret Units 3, 4 and 5 as estuarine or marine deposits, infilling localized coastal embayments that were flooded in advance of the regional transgression of the interfluves. Thus, the TS that separates marine above from nonmarine below must coalesce with I3 and go beneath Unit 3. The timing of the regional flooding is best recorded by FS2 that separates Unit 5 and 6 because the hiatus is minimized. FS1 is interpreted to be a local flooding surface that represents a period of rapid sea level rise separating Units 4 and 5. The lack of lateral fluvial deposition in Units 3, 4, and 5 indicates that this segment of the valley was predominantly undergoing erosion and sediment bypass during the downcutting of I-3 and I-4. High discharge events, such as meltwater outbursts during deglaciation, would scour the upper reaches of the channel, transporting the sediment farther offshore, and may explain the lack of fluvial fill observed in the subbottom data (Figs. 5–8).

The large constructional mound feature is elevated above Unit 2 and shows markedly different geometry than the strata beneath. The three dimensional morphology and internal downlapping stratigraphy suggest a constructional feature rather than an erosional remnant. The constructional mound is onlapped by both Units 3 and 4, suggesting that it may be associated with I-3/I-4 processes. The large size (~ 15 m high; 2 km wide), stratal geometry and sediment facies of the constructional mound is consistent with a fluvial origin, e.g. bar or braided island, in a high discharge environment. The constructional mound section of both JPC09 and JPC10 is comprised of well-sorted fine sand with small clay rip-up clasts on each of the downlapping surfaces (Fig. 12). The constructional mound pinches out to the NE and the sand recovered in JPC09 is slightly coarser than JPC10 sand from the upper part of the feature, suggesting the edges may be a lag deposit, with the finer sediment building up on the high. Geochemical analyses of JPC10 also indicate a relatively high percentage of organic carbon in the sandy constructional mound section, transitioning upward to very low organic content in Unit 6 (Lundeen, 2005), which points to a more terrestrial signal at the base overlain by marine sediment.

The marine shell dated at 13,500 yr BP in Unit 3 appears to be 1.24 m above I-3. Extrapolation with the sedimentation rate determined from JPC10 implies that I-3 was formed 14,300 yr BP, which coincides with Meltwater Pulse 1A (Fig. 16). In addition, evidence of a significant negative $\delta^{18}O$ excursion ~14,000 yr BP in cores from the Chukchi Borderland region is suggestive of meltwater input (Polyak et al., 2007). Thus we speculate I-3 was incised by meltwater discharge during post-LGM warming, with the open channel subsequently infilled by estuarine to marine sediment of Unit 3 (Figs. 5–8). Regional flooding of the interfluves across the Chukchi shelf, that is where Unit 6 overlies Unit 2 (Figs. 5 and 6) appears to correlate with FS1 (separating Unit 4/5) or FS2 (separating Unit 5/6) within the paleochannel, which implies that I-4 is older than the regional flooding (~11,500 yr BP), but younger than I-3. If correct then I-4 incision occurred ~12,000–13,000 yr BP, which also coincides with a second smaller negative $\delta^{18}O$ excursion found in cores from the Chukchi Borderland (Polyak et al., 2007). Evidence from a regionally extensive ice scour field on the outer Chukchi shelf suggests discharge of a large number icebergs, possibly sourced from the Chukchi margin of Alaska, during this time interval (Fig. 16) (Hill and Driscoll, 2006). Therefore, we speculate downcutting along I-4, which records a second phase of meltwater discharge, may be coincident with the release of the iceberg armada. The proposed timing of I-4 also correlates with deglaciation following a late stage glacial advance across the central and southwestern Brooks Range that ended ~11,500 ^{14}C yr BP (Hamilton, 1982, 1986). Since these most recent incisions appear to be unrelated to base level change, having occurred during a period of sea level rise, the I-3 and I-4 incision are not sequence boundaries formed by a base level fall. This evidence suggests that in glacially dominated landscapes, climatic factors can play an important role in creating incision and downcutting that is out of phase with sea level cycles.

5.3. Onshore and offshore drainage patterns

Structural controls from underlying bedrock may explain many of the drainage patterns observed across the Chukchi margin. Paleochannels incised into the Cretaceous strata appear to be controlled by cuestas and follow the strike of the underlying strata. Paleochannels and valleys mapped in this study appear to follow the same trend, flowing NNW along structural contours toward the shelf break and Chukchi borderland. The southern valley has been repeatedly excavated throughout multiple sea level cycles, creating the largest incised valley observed on the shelf. Drainage is concentrated in this region and flows axial parallel to the primary thrust of the Herald Arch, much like the Colville River onshore flows axial parallel to the Brooks Range. The Cretaceous strata outcrop at the seafloor near the southern valley, while the top of the Cretaceous strata is truncated beneath the modern seafloor in the north by as much as 25 m in some locations (Figs. 3 and 8). Drainage on the outer shelf appears directed along the strike of the Hanna wrench fault zone, but similar to the northern valley region, is relatively dispersed and does not appear to reoccupy the same valleys during subsequent sea level cycles. It appears that with increasing proximity to the Herald thrust belt, drainage is more strongly controlled by the underlying bedrock. This may explain why the southern valley is reoccupied during multiple sea level cycles.

Modern rivers draining the northwestern margin exhibit similar structural control. Satellite imagery of the Utukok and Kokolik Rivers shows meandering rivers with broad floodplains and numerous meander cutoffs, while the Kukpowruk River exhibits the least sinuosity and strongest bedrock control (Fig. 15). Profiles across portions of the Kokolik, Kukpowruk and Utukokok Rivers on the coastal plain bear out these observations. The Utukok and Kokolik Rivers exhibit much larger valleys than the Kukpowruk River, but appear to be less incised (Fig. 15). The Kukpowruk River is the closest of the three to the onshore extension of the Herald Thrust, which trends NNW across the Lisburne Peninsula (Fig. 2). Some authors have also speculated that neotectonic activity in the region may have influenced the course of the river (Cassavant and Miller, 2002).

The paleochannels and valleys observed in the nearshore region appear be much narrower and more distributed than their midshelf counterparts. This may be explained in part by sparse innershelf data coverage, the relatively poor resolution of many of the Boomer records in this region and the fact that many of the Boomer profiles trend parallel to the azimuth of the drainage. The midshelf may also be an

important drainage confluence as flows are constricted, passing between the broad structural highs of the Herald and Hanna Banks. The most landward profiles suggest that the southern valley may be split into two smaller valleys, a northern segment and a southern segment (Fig. 8). Based on acoustic character, the southern segment appears to contain predominantly Unit 2 deposits, while the northern segment is filled with Units 0 and 1, but shows no evidence of Unit 2. The two smaller valleys appear to converge, creating the much larger valley observed in CHIRP line 2 (Fig. 8).

Across the shelf, comparison of channel incisions relative to modern sea level, which takes into account differing modern seafloor elevations by normalizing all of the data points to a common baselevel, indicates there may be a knickpoint landward of the large incised valleys observed on the midshelf. With a few exceptions, channels and valleys imaged on the innershelf exhibit a base of incision around 55 m below modern sea level; this increases considerably to 85–100 m on the midshelf (Fig. 10). This suggests that the incised valleys on the midshelf may have been migrating shoreward through headward erosion as they attempted to regrade following base level lowering. The knickpoint on the midshelf at ~40–45 m water depth may indicate the point beyond which fluvial rejuvenation of the system and farther landward incision was restricted. Thus it appears that a combination of headward erosion and drainage confluence may have contributed to the misfit of the large midshelf incised valleys relative to smaller channels and valleys observed on the midshelf. Unfortunately, a lack of additional data makes it difficult to fully constrain the extent of the incised valleys across the shelf or to ascertain how the individual channels correlate with various sea level cycles.

Drainage observed in the nearshore region appears to emanate from two sources on the northwestern Alaskan margin and may link modern rivers with the larger incised valleys observed on the midshelf. One set may represent the paleo-Kokolik/Kukpowruk channels that connect to the southern valley, while the other set appears to flow between the Utukok River and the northern valley region (Fig. 4). The modern rivers draining the northwestern margin of Alaska (Figs. 1 and 15) have very low discharge and relatively small drainage areas that suggest a misfit with the offshore drainage. Nevertheless, these rivers have steep banks and incised channel morphologies cut into the Brooks Range foothills, which suggest that they may have been carved by much stronger flows in the past (Fig. 15). The dimensions of these northwestern river valleys are less than half the size of the valleys defined by I-3 or I-4 on the midshelf. The lack of fluvial fill in the I-3 and I-4 valleys makes it difficult to compare the offshore channel networks with the northwestern rivers. The onshore river valleys may be more deeply incised than they appear in the profiles since we were not able to measure unfilled valley dimensions. The northwestern river valleys were most likely carved by the same processes as on the midshelf, but are filled with fluvial sequences emplaced within the last 8000 yr, as the rate of sea level rise slowed and channels were able to regrade (Fig. 16).

5.4. Climate

The presence of glacial meltwater channels on the shelf implies a greater extent of glaciation in northwestern Alaska during the LGM than previously recognized. While the mapped extent of glaciation at this time is largely restricted to the central and eastern Brooks Range, some highland glaciation also been mapped in the southern Brooks Range foothills (Fig. 1). Throughout recent glacial periods ice masses repeatedly dammed the headwaters of the Noatak River, creating a succession of proglacial lakes, collectively termed Glacial Lake Noatak (Fig. 17) (Hamilton, 2001, 2003). The northern margin of this ice dammed lake was located just south of the western Brooks Range drainage divide. The headwaters of the northwestern rivers are located 15–20 km to the north of LGM age glacial lake deposits (Fig. 17). While very few field studies have been conducted along the

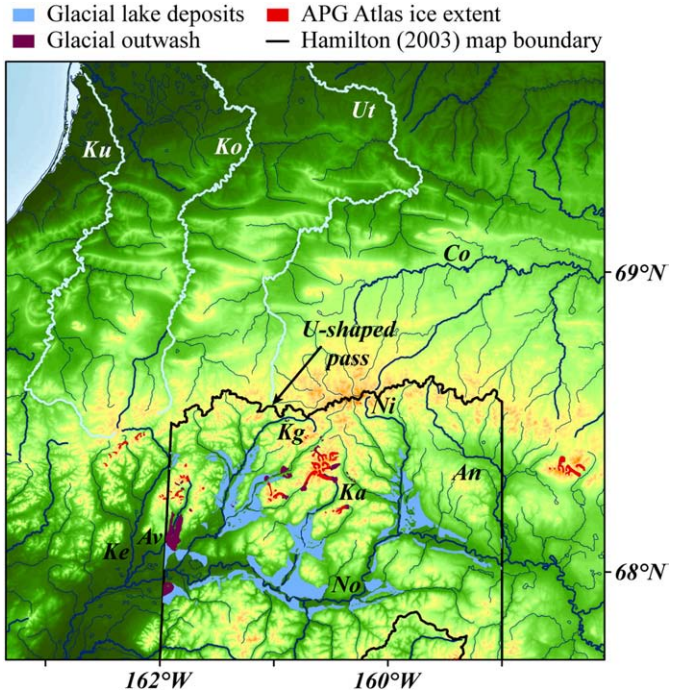

Fig. 17. Map of western Brooks Range showing the mapped extent of Glacial Lake Noatak deposits from the LGM (Hamilton, 2003). Also shown is the Alaska Paleoglacier Atlas LGM age ice extent for the region. The thick black line denotes the boundary of the Hamilton (2003) map. Note the close proximity of the Glacial Lake Noatak to the headwaters of the northwestern rivers. Abbreviations are as follows: Ku — Kukpowruk River, Ko — Kokolik River, Ut — Utukok River, Co — Colville River, Ke — Kelly River, Av — Avan River, Ka — Kaluktavik River, Ni — Nimiutuk River, An — Anisak River.

northwestern rivers, hydrologic reconnaissance reports from the 1950s of the northwestern foothills indicates the presence of stream incised U-shaped valleys and north facing cirques across the region encompassing the Utukok, Kokolik and Kukpowruk headwaters (Sable et al., 1981). These features are tentatively attributed to older glaciations; however, it appears plausible that glacial lake damming similar to the Noatak region may have occurred on the northern side of the drainage divide as well. Geologic mapping in the Noatak region indicates the presence of a U-shaped pass of unspecified age where glaciers flowed north from the edge of the interpreted region into the Utukok River headwaters (Fig. 17) (Hamilton, 2003). Hamilton (2003) suggested that Glacial Lake Noatak water levels commonly fluctuated throughout glaciation, leaving behind weakly developed shoreline features that are difficult to trace. Additionally, the underlying geology of the northwestern foothills is very different from the Noatak region, making it difficult to compare morphologies on the basis of DEMs alone and highlights the need for field mapping in the region.

The primary argument for limited Brooks Range glaciation during the LGM often focuses on a synoptic paleoclimate record for the region that emphasizes a lack of moisture necessary for significant ice buildup (e.g. Brigham-Grette, 2001). While it is likely that the general paleoclimatic trend of northern Alaska was toward exceptionally aridity during the LGM, some studies have suggested that there may have been considerable spatial heterogeneity (e.g., Mock and Anderson, 1997; Edwards et al., 2001). Hamilton (2003) documented evidence of an “unusually large valley glacier” in the Avan River valley during the LGM and speculates that the Avan region, which is in close proximity to headwaters of the Kokolik and Kukpowruk Rivers (Fig. 17), must have been experiencing much higher snow fall at this time than the highlands to the east. This example highlights the role of small scale regional variability in moisture conditions across the northwestern margin during the LGM and implies similar paleoclimatic conditions may have also existed across the headwaters of the

northwestern rivers. The evidence presented here for glacial meltwater drainage on the shelf does not necessarily suggest large ice sheets across the region, but rather indicates that there may have been more extensive alpine glaciation during the LGM than previously recognized.

5.5. Sea level and Holocene sedimentation

Extrapolation of sedimentation in several of the midshelf cores allows us to place some new constraints on the timing of sea level rise across the Chukchi margin. The age of TS in JPC02 indicates marine inundation of the Hope Valley and nearby Bering Strait occurred ~12,000 yr BP (Figs. 13 and 16), nearly 1000 yr earlier than previous estimates (Elias et al., 1996; Keigwin et al., 2006). The estimated age of TS in both JPC09 and JPC10 from the southern valley suggests that this surface represents rapid flooding across the Chukchi midshelf ~11,500 yr BP and may correlate with globally recognized Meltwater Pulse 1-B (Figs. 12 and 16) (Bard et al., 1996).

Sediment cores and CHIRP subbottom data from the mid to outer shelf show evidence of a prominent flooding surface (FS) near the base of Unit 6 (Fig. 14). In some instances the core locations are projected >100 m; however, these correlations appear reasonable given that the subbottom data coverage indicates that the cores collected sediments from regionally extensive horizons, and all of the cores in this region exhibit similar stratigraphy. Akin to the flooding surface transitions observed across the southern valley, each of the sediment cores exhibits a distinct shift in grain size from sand or interbedded sand and silt to silty clay at the FS boundary (Fig. 14). The coarser grains appear to represent a lag deposit accumulated during the flooding and wave-base reworking, followed by finer-grained sediment deposition above as the shoreline and associated facies migrates landward. While the age of the FS boundary is unknown, the paleodepth of the surface is roughly the same in each of the sediment cores. Plotting this surface on the global sea level curve and assuming it is marine allow us to place some constraints on the maximum age of the surface. The mid to outer shelf FS is at the same paleodepth as the regional transgressive surface (TS) observed across the southern incised valley and Hope Valley. This suggests that FS may represent the transgressive surface across this portion of the shelf, corresponding to Meltwater Pulse-1B (Fig. 16). If the midshelf FS is younger, it most likely formed within several meters of the transgression and may represent a younger episode of rapid sea level rise.

Radiocarbon dating from cores in both the Hope Valley (JPC02) and the midshelf (JPC10) suggests that the sedimentation rate across the Chukchi shelf was relatively high during the rapid sea level rise following the LGM, and decreased dramatically ~7000 yr BP. Between 11 ka and 7 ka, portions of the Hope Valley accumulated as much as 10 m of Holocene sediment, with almost no sedimentation thereafter (Fig. 13). This is unusual, given that sequence stratigraphic models commonly predict sediment starvation on the shelf during rapid sea level rise as the margin becomes inundated and sediment is trapped in shallow embayments (Vail, 1987; Van Wagoner et al., 1990). Typically, as the rate of sea level rise begins to slow, we would expect sediment accumulation rates to slowly increase. This prediction is borne out in other river deltas around the world (Stanley and Warne, 1994), many of which show a prominent build out around 8000 yr BP, as the rate of sea level began to slow (Fairbanks, 1989). In contrast, sedimentation on the Chukchi margin appears to be highest during the rapid sea level rise, which suggests that there must have been additional inputs. Precipitation and moisture levels across the continent began to increase during deglaciation, as sea level rise flooded the shelf and brought moister maritime climates to the region (Edwards et al., 2001); however, paleoprecipitation was still 10–20% less than modern 6000 yr BP (Barber and Finney, 2000). Pluvial conditions during deglaciation may have increased glacial water storage and led to glacial readvances observed in the central and southwestern Brooks Range between 13,000 and 11,500 ^{14}C yr BP (Hamilton, 1986). Increased moisture input would have also augmented glacial meltwater discharge, which would have maintained high sediment input during this period. The drop in sedimentation roughly coincides with the global cessation of meltwater discharge ~8 ka (Barber et al., 1999). Despite uncertainties derived from the small number of data points, unknowns surrounding the exact radiocarbon reservoir age, and the correlation of cores and subbottom data across large distances, this evidence suggests that local meltwater pulses to the Chukchi margin may be in phase with global meltwater patterns and provides an intriguing set of initial results that may facilitate more research.

6. Conclusions

The Chukchi shelf appears to have been an important drainage pathway during periods of lowered sea level, as evidenced by the numerous paleochannels and valleys observed on the mid to outer shelf. This is contrary to the assertion that most of the flow across the Chukchi was derived from the Hope Valley and escaped down the Herald Canyon offshore, largely bypassing the greater shelf region (McManus et al., 1983). The southern incised valley shows evidence of multiple incisions, representing sequence boundaries that correlate with periods of lowered sea level, possibly as recent as the LGM. Sequence stratigraphic models for siliciclastic margins generally predict fluvial incision during the falling limb of sea level, as base level lowering leads to stream rejuvenation (Christie-Blick and Driscoll, 1995). In contrast, the two most recent incisions, I-3 and I-4, appear to have been downcut during the period of sea level rise following the LGM, and therefore do not represent sequence boundaries but rather are related to important climatic events. This evidence suggests that on glaciated margins it is important to realize that not all incisions represent sequence boundaries. In these cases, the timing of channel excavation and nature of the fill is very important in determining whether the incision is related to base level change or climatically driven.

Sea level records across the shelf indicate that the regional transgression occurred 11,500 to 12,000 yr BP, coincident with Meltwater Pulse 1-B. Following transgression, shelf sedimentation appears to have remained unusually high throughout deglaciation and rapid sea level rise, most likely the result of the large volumes of fresh water input from melting glaciers following the LGM. The meltwater drainage observed on the shelf may have been derived from glacial lake breaching; regardless it highlights the role of climatic heterogeneity across the region and implies a greater extent of continental glaciation during the LGM than previously proposed.

Acknowledgements

This research was supported by a grant from the NSF Office of Polar Programs. We would like to thank R. Lawrence Phillips of the U.S. Geological Survey for his contributions, which include participating in the research cruise, providing additional data and thoughtful discussions.

References

Aagaard, K., Carmack, E., 1989. The role of sea ice and other fresh water in the Arctic circulation. J. Geophys. Res. 94, 14485–14498.

Barber, D.C., Dyke, A., Hillaire-Marcel, C., Jennings, A.E., Andrews, J.T., Kerwin, M.W., Bilodeau, G., McNeely, R., Southon, J., Morehead, M.D., Gagnonk, J.-M., 1999. Forcing of the cold event of 8,200 years ago by catastrophic drainage of Laurentide lakes. Nature 400, 344–348.

Barber, V.A., Finney, B.P., 2000. Late Quaternary paleoclimatic reconstructions for interior Alaska based on paleolake-level data and hydrologic models. J. Paleolimnol. 24, 29–41.

Bard, E., Hamelin, B., Arnold, M., Montaggioni, L., Cabioch, G., Faure, G., Rougerie, F., 1996. Deglacial sea level record from Tahiti corals and the timing of global meltwater discharge. Nature 382, 241–244.

Bondevik, S., Birks, H., Gulliksen, S., Mangerud, J., 1999. Late Weichselian marine ^{14}C reservoir ages at the western coast of Norway. Quat. Res. 52, 104–114.

Bretz, J.H., 1969. The Lake Missoula floods and the Channeled Scabland. J. Geol. 77, 505–543.
Brigham-Grette, J., 2001. New perspectives on Beringian Quaternary paleogeography, stratigraphy and glacial history. Quat. Sci. Rev. 20, 15–24.
Brigham-Grette, J., Lozhkin, A.V., Anderson, P.M., Glushkova, O.Y., 2004. Paleoenvironmental conditions in western Beringia before and during the Last Glacial Maximum. In: Madsen, D.B. (Ed.), Entering America: Northeast Asia and Beringia Before the Last Glacial Maximum. University of Utah Press, Salt Lake City, pp. 29–61.
Cassavant, R.R., Miller, S.R., 2002. Tectonic geomorphic characterization of a transcurrent fault zone, western Brooks Range, Alaska. AAPG Bulletin 86, 1139.
Chappell, J., Shackleton, N.J., 1986. Oxygen isotopes and sea level. Nature 324, 137–140.
Childers, J.M., Kernodle, D.R., Loeffler, R.M., 1979. Hydrologic reconnaissance of western Arctic Alaska, 1976 and 1977. U.S. Geological Survey Open-File Report 79-699.
Christie-Blick, N., Driscoll, N.W., 1995. Sequence stratigraphy. Ann. Rev. Earth Planet. Sci. 25, 451–478.
Cohen, J.K., Stockwell Jr., J.W., 1999. CWP/SU: Seismic Unix Release 33: a Free Package for Seismic Research and Processing. Center for Wave Phenomena, Colorado School of Mines.
Cook, M.S., Keigwin, L.D., Sancetta, C.A., 2005. The deglacial history of surface and intermediate water of the Bering Sea. Deep Sea Res. II 52, 2163–2173.
Dalrymple, R.W., Boyd, R., Zaitlin, B.A. (Eds.), 1994. Incised-Valley Systems: Origin and Sedimentary Sequences. Society for Sedimentary Geology Special Publication, vol. 51. 391 pp.
Donnelly, J.P., Driscoll, N.W., Uchupi, E.A., Keigwin, L.D., Schwab, W.C., Thieler, E.R., Swift, S.A., 2005. Catastrophic meltwater discharge down the Hudson Valley: a potential trigger for the Intra-Allerød cold period. Geology 33, 89–92.
Edwards, M.E., Mock, C.J., Finney, B.P., Barber, V.A., Bartlein, P.J., 2001. Potential analogues for paleoclimatic variations in eastern interior Alaska during the past 14,000 yr: atmospheric-circulation controls of regional temperature and moisture response. Quat. Sci. Rev. 20, 189–202.
Elias, S.A., Short, S.K., Nelson, C.H., Birks, H.H., 1996. Life and times of the Bering land bridge. Nature 382, 60–63.
Fairbanks, R.G., 1989. A 17,000-year glacio-eustatic sea level record; influence of glacial melting rates on the Younger Dryas event and deep-ocean circulation. Nature 342, 637–642.
Fairbanks, R.G., 1990. The age and origin of the "Younger Dryas climate event" in Greenland ice cores. Paleoceanography 5, 937–948.
Fairbanks, R.G., Mortlock, R.A., Tzu-Chien, C., Cao, L., Kaplan, A., Guilderson, T., Fairbanks, T.W., Bloom, A.L., 2005. Marine radiocarbon calibration curve spanning 0 to 50,000 years B.P. based on paired $^{230}Th/^{234}U/^{238}U$ and ^{14}C dates on pristine corals. Quat. Sci. Rev. 24, 1781–1796.
Forman, S.L., Polyak, L., 1997. Radiocarbon content of pre-bomb marine mollusks and variations in the ^{14}C reservoir age for coastal areas of the Barents and Kara Seas, Russia. Geophys. Res. Lett. 24, 885–888.
Grosswald, M.G., Hughes, T.J., 2002. The Russian component of an Arctic ice sheet during the Last Glacial Maximum. Quat. Sci. Rev. 21, 121–146.
Grosswald, M.G., Hughes, T.J., 2004. Chlorine-36 and ^{14}C chronology support a limited last glacial maximum across central Chukotka, northeastern Siberia, and no Beringian ice sheet; discussion. Quat. Res. 62, 223–226.
Hamilton, T.D., 1982. A late Pleistocene glacial chronology for the southern Brooks Range: stratigraphic record and regional significance. GSA Bulletin 93, 700–716.
Hamilton, T.D., 1986. Late Cenozoic glaciation of the central Brooks Range. In: Hamilton, T.D., Reed, K.M., Thorson, R.M. (Eds.), Glaciation in Alaska: The Geologic Record. Alaska Geological Society, pp. 9–50.
Hamilton, T.D., 2001. Quaternary, glacial, lacustrine, and fluvial interactions in the western Noatak Basin. Quat. Sci. Rev. 20, 371–391.
Hamilton, T.D., 2003. Surficial geologic map of parts of the Misheguk Mountain and Baird Mountain quadrangles, Noatak National Preserve, Alaska. U.S. Geological Survey Open-File Report 03-367.
Henkart, P., 2006. SIOSEIS. http://sioseis.ucsd.edu.
Hill, J.C., Driscoll, N.W., 2006. Incision and Downcutting on Glaciated Margins: Out of Phase with Sea Level Cycles? NSF MARGINS TEI: Teleconnections Between Source and Sink in Sediment Dispersal Systems, 17–21 September 2006.
Hill, J.C., Driscoll, N.W., Brigham-Grette, J., Donnelly, J.P., Gayes, P.T., Keigwin, L.D., 2007. New evidence for high discharge to the Chukchi shelf during the Last Glacial Maximum. Quat. Res. 68, 271–279.
Jakobsson, M., Gardner, J.V., Vogt, P.R., Mayer, L.A., Armstrong, A., Backman, J., Brennan, R., Calder, B., Hall, J.K., Kraft, B., 2005. Multibeam bathymetric and sediment profiler evidence for ice grounding on the Chukchi Bordlerland, Arctic Ocean. Quat. Res. 63, 150–160.
Keigwin, L.D., Donnelly, J.P., Cook, M.S., Driscoll, N.W., Brigham-Grette, J., 2006. Rapid sea-level rise and Holocene climate in the Chukchi Sea. Geology 34, 861–864.
Lamke, R.D., Brabets, T.P., McIntire, J.A., 1995. Hydrologic Unit Codes (HUC) for State of Alaska. U.S. Geological Survey.
Lundeen, Z., 2005. Elemental and isotopic constraints on the late glacial–Holocene transgression and paleoceanography of the Chukchi Sea. M.S. Thesis, University of Massachusetts Amherst.
Manley, W.F., 2001. Alaska North Slope 100 m Digital Elevation Model (DEM). National Snow and Ice Data Center. Boulder, CO.
Manley, W.F., Kaufman, D.S., 2002. Alaska PaleoGlacier Atlas, v. 1. Institute of Arctic and Alpine Research (INSTAAR). University of Colorado.
McManus, D.A., Creager, J.S., Echols, R.J., Holmes, M.L., 1983. The Holocene transgression of the flank of Beringia: Chukchi valley to Chukchi estuary to Chukchi Sea. In: Masters, P.M., Flemming, N.C. (Eds.), Quaternary Coastlines and Marine Archaeology: Towards the Prehistory of Land Bridges and Continental Shelves. Academic Press, London, pp. 365–388.
Miley, J.M., Barnes, P.W., 1986. 1985 Field studies. Beaufort and Chukchi Seas, conducted from the NOAA Ship Discoverer. U.S. Geological Survey Open-File Report 86-202.
Mock, C.J., Anderson, P.M., 1997. Some perspectives on the late Quaternary paleoclimate of Beringia. In: Isaacs, C.M., Tharp, V.L. (Eds.), Proceedings of the Thirteenth Annual Pacific Climate (PACLIM) Workshop.
Moore, T.E., Dumitru, T.A., Adams, K.E., Witebsky, S.N., Harris, A.G., 1994. Origin of the Lisburne Hills–Herald Arch structural belt: stratigraphic, structural, and fission-track evidence from the Cape Lisburne area, northwestern Alaska. In: Miller, E.L., Grantz, A., Klemperer, S.L. (Eds.), Tectonic Evolution of the Bering Shelf–Chukchi Sea–Arctic Margin and Adjacent Landmasses. Geological Society of America, pp. 77–109. Special Paper 360.
Moore, T.E., Wallace, W.K., Bird, K.J., Karl, S.M., Mull, C.G., Dillon, J.T., 2002. Geology of northern Alaska. In: Pflaker, G., Berg, H.C. (Eds.), The Geology of Alaska. Geological Society of America, Boulder, pp. 49–140.
Normark, W.R., Reid, J.A., 1998. Extensive deposits on the Pacific plate from late Pleistocene North American glacial lake outbursts. J. Geol. 111, 617–637.
Phillips, R.L., Pickthorn, L.G., Rearic, D.M., 1987. Late Cretaceous sediments form the northeast Chukchi Sea. In: Galloway, J.P., Hamilton, T.D. (Eds.), Geologic Studies in Alaska by the U.S. Geological Survey during 1987. U.S. Geological Survey Circular, vol. 1016, pp. 187–189.
Phillips, R.L., Barnes, P., Huner, R.E., Reiss, T.E., Rearic, D.M., 1988. Geologic investigations in the Chukchi Sea, 1984, NOAA ship SURVEYOR cruise. U.S. Geological Survey Open-File Report 88-25.
Polyak, L., Edwards, M.E., Coakley, B.J., Jakobsson, M., 2001. Ice shelves in the Pleistocene Arctic Ocean inferred from glaciogenic deep-sea bedforms. Nature 410, 453–457.
Polyak, L., Darby, D.A., Bischof, J.F., Jakobsson, M., 2007. Stratigraphic constraints on late Pleistocene glacial erosion and deglaciation of the Chukchi margin. Arctic Ocean. Quat. Res. 67, 234–245.
Sable, E.G., Dutro, J.T., Mangus, M.D., Morris, R.H., 1981. Geology of the Kukpowruk-Nuka region, northwestern Alaska. U.S. Geological Survey Open-File Report 81-1078.
Schumm, S.A., Mosley, M.P., Weaver, W.E., 1987. Experimental Fluvial Geomorphology. Wiley, New York. 413 pp.
Smith, L.M., Miller, G.H., Otto-Bliesner, B., Shin, S.-I., 2003. Sensitivity of the Northern Hemisphere climate system to extreme changes in Holocene Arctic sea ice. Quat. Sci. Rev. 22, 645–658.
Stanley, D.J., Warne, A.G., 1994. Worldwide initiation of Holocene marine deltas by deceleration of sea-level rise. Science 265, 228–231.
Stuiver, M., Grootes, P.M., 2000. GISP2 oxygen isotope ratios. Quat. Res. 53, 277–284.
Thurston, D.K., Theiss, L.A., 1987. Geologic report for the Chukchi Sea planning area, Alaska. U.S. Dept. of the Interior Minerals Management Service OCS Report MMS 87-0046.
Tolson, R.B., 1987. Structure and stratigraphy of the Hope Basin, southern Chukchi Sea, Alaska. In: Scholl, D.W., Grantz, A., Vedder, J.G. (Eds.), Geology and Resource Potential of the Continental Margin of Western North America and Adjacent Ocean Basins, Beaufort Sea to Baja California, pp. 59–71.
Uchupi, E., Driscoll, N., Ballard, R.D., Bolmer, S.T., 2001. Drainage of late Wisconsin glacial lakes and the morphology and late quaternary stratigraphy of the New Jersey–southern New England continental shelf and slope. Mar. Geol. 172, 117–145.
Vail, P.R., 1987. Seismic stratigraphy interpretation utilizing sequence stratigraphy. In: Bally, A.W. (Ed.), Atlas of Seismic Stratigraphy. American Association of Petroleum Geologists, Tulsa, pp. 1–10.
Van Wagoner, J.C., Mitchum, R.M., Campion, K.C., Rahmanian, V.D., 1990. Siliciclastic Sequence Stratigraphy in Well Logs, Cores and Outcrops: Concepts for High-Resolution Correlation of Time and Facies. American Association of Petroleum Geologists, Tulsa. 55pp.
Zaitlin, B.A., Dalrymple, R.W., Boyd, R., 1994. The stratigraphic organization of incised-valley systems associated with relative sea-level changes. In: Dalrymple, R.W., Boyd, R., Zaitlin, B.A. (Eds.), Incised-Valley Systems: Origin and Sedimentary Sequences. Society for Sedimentary Geology Special Publication, vol. 51, pp. 45–59. Tulsa.
Zuffa, G.G., Normark, W.R., Serra, F., Bruner, C.A., 2000. Turbidite megabeds in an oceanic rift valley recording Jökulhaups of Late Pleistocene glacial lakes of the Western United States. J. Geol. 108, 253–274.
Zweck, C., Huybrechts, P., 2005. Modelling of the northern hemisphere ice sheets during the last glacial cycle and glaciological sensitivity. J. Geophys. Res. 110. doi:10.1029/2004JD005489.